NeuroImage: Clinical 37 (2023) 103277

Contents lists available at ScienceDirect

NeuroImage: Clinical

journal homepage: www.elsevier.com/locate/ynicl

Spectral slowing in chronic stroke reflects abnormalities in both periodic and aperiodic neural dynamics

Phillip R. Johnston [a,b,*], Anthony R. McIntosh [c,d], Jed A. Meltzer [a,b,e]

[a] Department of Psychology, University of Toronto, 100 St. George Street, Toronto, ON M5S 3G3, Canada
[b] Rotman Research Institute, Baycrest Health Sciences, 3560 Bathurst Street, Toronto, ON M6A 2E1, Canada
[c] Biomedical Physiology and Kinesiology, Simon Fraser University, 8888 University Drive E K9625, Burnaby, BC V5A 1S6, Canada
[d] Institute for Neuroscience and Neurotechnology, Simon Fraser University, 8888 University Drive E K9625, Burnaby, BC V5A 1S6, Canada
[e] Department of Speech-Language Pathology, University of Toronto, 500 University Avenue, Toronto, ON M5G 1V7, Canada

ARTICLE INFO

Keywords:
Stroke
Magnetoencephalography
Spectral slowing
Spectral parameterization
Aperiodic dynamics
1/f scaling

ABSTRACT

Decades of electrophysiological work have demonstrated the presence of "spectral slowing" in stroke patients – a prominent shift in the power spectrum towards lower frequencies, most evident in the vicinity of the lesion itself. Despite the reliability of this slowing as a marker of dysfunctional tissue across patient groups as well as animal models, it has yet to be explained in terms of the pathophysiological processes of stroke. To do so requires clear understanding of the neural dynamics that these differences represent, acknowledging the often overlooked fact that spectral power reflects more than just the amplitude of neural oscillations. To accomplish this, we used a combination of frequency domain and time domain measures to disambiguate and quantify periodic (oscillatory) and aperiodic (non-oscillatory) neural dynamics in resting state magnetoencephalography (MEG) recordings from chronic stroke patients. We found that abnormally elevated low frequency power in these patients was best explained by a steepening of the aperiodic component of the power spectrum, rather than an enhancement of low frequency oscillations, as is often assumed. However, genuine oscillatory activity at higher frequencies was also found to be abnormal, with patients showing alpha slowing and diminished oscillatory activity in the beta band. These aperiodic and periodic abnormalities were found to covary, and could be detected even in the un-lesioned hemisphere, however they were most prominent in perilesional tissue, where their magnitude was predictive of cognitive impairment. This work redefines spectral slowing as a pattern of changes involving both aperiodic and periodic neural dynamics and narrows the gap in understanding between non-invasive markers of dysfunctional tissue and disease processes responsible for altered neural dynamics.

1. Introduction

Electrophysiological methods have been employed in stroke diagnosis and research for the better part of a century. Across this large literature, the predominant finding is that stroke patients exhibit abnormally elevated "slow" activity, particularly in the vicinity of the lesion itself (e.g. Ahmed, 1988; Cohn et al., 1948; Laaksonen et al., 2013; Leemburg et al., 2018; Murri et al., 1998; Nagata et al., 1982; Tecchio et al., 2005). This elevated activity, typically quantified as increased spectral power in the delta band (from 1–3 or 1–4 Hz), is detectable across electrophysiological modalities in both acute and chronic patients, as well as animal models, and appears to be a marker of tissue dysfunction and related impairment (e.g. Assenza et al., 2009; Laaksonen et al., 2013; Meinzer et al., 2008; Tecchio et al., 2007; Zappasodi et al., 2007). Despite the robustness of this effect, the pathophysiological processes responsible are unknown, and therefore prospects for rehabilitating chronically affected tissue are uncertain. Furthermore, it is unclear whether additional abnormal features sometimes observed in stroke, such as diminished high frequency (beta/gamma) power (Chu et al., 2015; Kielar et al., 2016; Shah-Basak et al., 2020; Tecchio et al., 2005; van Wijngaarden et al., 2016; Wu et al., 2016), share the same underlying cause (suggesting a unitary spectral "slowing"), or instead

Abbreviations: MEG, magnetoencephalography; EXP, aperiodic exponent; BCF, beta center frequency; BPW, beta power; BBW, beta bandwidth; TACF, theta-alpha center frequency; TAPW, theta-alpha power; TABW, theta-alpha bandwidth; DLC, delta lagged coherence; TALC, theta-alpha lagged coherence; BLC, beta lagged coherence.

* Corresponding author at: Rotman Research Institute, Baycrest Health Sciences, 3560 Bathurst Street, Toronto, ON M6A 2E1, Canada.
E-mail address: pjohnston@research.baycrest.org (P.R. Johnston).

https://doi.org/10.1016/j.nicl.2022.103277
Received 16 September 2022; Received in revised form 21 November 2022; Accepted 30 November 2022
Available online 1 December 2022

reflect additional complications of the disease.

Understanding the cause of such abnormal spectral features, and potentially how to normalize them, requires a clear picture of the neural dynamics they represent. Throughout the literature, and especially since the advent of spectral analysis in stroke electrophysiology, this abnormal slow activity has typically been interpreted to reflect increased amplitude of slow neural oscillations, as suggested by terms such as "rhythms" or "waves", if not stated explicitly. This implies that stroke dysfunction is related to synchronized, rhythmic fluctuation of membrane potentials across large groups of neurons, such as those observed during slow wave sleep (Destexhe et al., 1999). However, this interpretation is not justified, as spectral representations cannot distinguish between periodic (i.e. oscillatory, rhythmic) and aperiodic (i.e. transient, non-rhythmic) processes (Donoghue et al., 2021; He, 2014; Pritchard, 1992). As such, presence of, or change in, neural oscillations cannot be inferred from spectral power alone, nor from the amplitude of band-limited signals (Donoghue et al., 2021).

This conflation of the aperiodic and periodic components raises the possibility that the elevated low frequency power in stroke is, in fact, aperiodic in nature. While genuine neural oscillations produce narrow peaks in the power spectrum, aperiodic activity produces a broadband component spanning the entire spectrum, with power rapidly falling off at higher frequencies. More concretely, the aperiodic component tends to follow a power law function: $P \propto 1/f^{\beta}$, where P is power, f is frequency, and β is the 'aperiodic exponent', which determines how steeply power decreases as frequency increases. Therefore, the enhanced low frequency power observed in stroke patients could instead reflect a "rotation" of the aperiodic component towards lower frequencies and away from higher frequencies. This rotation, quantified by an increase in the aperiodic exponent β, would instead point to a prominent disruption of aperiodic rather than oscillatory processes in stroke. Indeed, there is already some preliminary evidence for a steepening of the aperiodic slope in animal stroke models (Leemburg et al., 2018) and scalp EEG in human patients (Lanzone et al., 2022), and a rotation of the aperiodic background would also explain why the ratio of low frequency to high frequency spectral power has been a successful measure in clinical prognosis (Finnigan and van Putten, 2013). However, there is still a possibility that true differences in neural oscillations (e.g. a high amplitude oscillation at the lower end of the fitting range; Gerster et al., 2021) could produce the same pattern of results.

To adjudicate between these possibilities, we used both frequency and time domain measures to disentangle the aperiodic and periodic components of resting-state magnetoencephalography (MEG) signals from chronic stroke patients. Specifically, we applied *specparam* (Donoghue et al., 2020), an algorithm that explicitly models and quantifies the aperiodic ($1/f^{\beta}$ background) and periodic component (narrowband peaks) derived from the power spectrum. Looking beyond spectral power, we also applied lagged coherence (Fransen et al., 2015), which quantifies the rhythmicity of the signal in the time domain, providing a complementary measure of periodic activity, if present. By combining these methods, we were able to determine whether elevated low frequency power is attributable to periodic or aperiodic processes, and provide a much more complete characterization of any additional abnormalities in stroke than is currently available. Additionally, we investigated the spatial distribution of these abnormalities by localizing MEG signals to their cortical sources. Our primary focus was tissue in the vicinity of the lesion itself (perilesional tissue), which is known to demonstrate the most prominent electrophysiological abnormalities, but also examined how areas more distant to the lesion, particularly the unlesioned hemisphere, also exhibit abnormal activity, reflecting the notion of 'diaschisis' (Feeney and Baron, 1986; Finger et al., 2004). Together, these are critical steps towards more precisely-defined, reliable markers of dysfunctional tissue, that provide new insight into underlying neural dynamics, facilitating physiological interpretation and potentially rehabilitation.

2. Methods

2.1. Participants

Our sample included twenty-three chronic stroke patients (seventeen men, six women) drawn from two prior studies (Kielar et al., 2016; Shah-

Table 1
Stroke patient demographic and lesion characteristics. See Kielar et al. (2016) and Shah-Basak et al. (2020) for further information.

Patient	Cohort	Age (years)	Education (years)	Sex	Handedness	Time post-onset	Etiology	Lesion volume (mm^3)	% brain volume lesioned
P1	Kielar	67	21	M	R	15y 6 m	Hemorrhagic	217,065	13.76
P2	Kielar	70	24	M	R	1y	Ischemic	2952	0.21
P3	Kielar	75	15	M	R	2y 5 m	Ischemic	48,137	2.54
P4	Kielar	79	10	M	R	2y 1 m	Ischemic	32,901	2.44
P5	Kielar	46	15	M	R	2y 3 m	Ischemic	30,861	2.20
P6	Kielar	62	16	M	R	1y 2 m	Ischemic	38,064	2.61
P7	Kielar	84	19	M	R	10y	Ischemic	4501	0.29
P8	Kielar	73	19	M	L	5y 8 m	Hemorrhagic	21,589	1.48
P9	Kielar	77	20	M	R	7 m	Ischemic	22,910	1.38
P10	Kielar	66	20	M	R	5y 3 m	Unspecified	81,473	5.86
P11	Kielar	46	16	M	R	4y	Ischemic	99,098	6.71
P12	Kielar	57	12	M	R	2y	Unspecified	115,811	8.81
P13	Kielar	65	20	M	R	7y 1 m	Ischemic	177,022	12.72
P14	Kielar	60	14	F	R	8y 8 m	Unspecified	84,290	6.23
P15	Kielar	69	15	M	R	1y	Ischemic	7645	0.57
P16	Kielar	68	13	F	R	3y 4 m	Hemorrhagic	21,796	1.81
P17	Kielar	68	14	F	R	5y 6 m	Hemorrhagic	45,874	3.24
P18	Shah-Basak	61	16	M	R	4y	Ischemic	27,118	2.05
P19	Shah-Basak	34	19	F	R	4y	Ischemic	21,004	1.55
P20	Shah-Basak	41	18	M	R	5y 9 m	Ischemic	50,942	3.90
P21	Shah-Basak	75	18	F	R	2y 1 m	Ischemic	7012	0.54
P22	Shah-Basak	68	16	M	R	4y 10 m	Hemorrhagic	10,165	0.67
P23	Shah-Basak	46	18	F	R	4y 2 m	Unspecified	36,942	2.94
Mean (SD)		63.35 (12.98)	16.87 (3.24)			4.56y (3.51y)			3.67 (3.75)

Basak et al., 2020), with an average age of 63.4 years (SD = 13.0 years), and 16.9 years (SD = 3.24 years) of education. All patients had a single left-hemispheric stroke (mostly ischemic, see Table 1) at least six months prior to data collection (average time post onset = 4.6 years, SD = 3.5 years), and demonstrated symptoms of aphasia. All patients were right-handed except one. See Table 1 for further details.

Patients were matched for age ($t(44) = -1.028$, $p = 0.310$) and education ($t(44) = -0.928$, $p = 0.358$) with a sample of twenty-three healthy control participants (seventeen men, six women) from the same studies as above. Control participants had a mean age of 66.9 years (SD = 10.4), and 17.7 years (SD = 2.4) of education.

All data collection took place at the Rotman Research Institute in Toronto, Canada, and was approved by the Research Ethics Board at Baycrest Health Sciences. All participants gave written informed consent and were compensated for their participation. For further details about recruitment and exclusion criteria, see Kielar et al. (2016) and Shah-Basak et al. (2020).

2.2. Structural MRI acquisition and processing

A T1-weighted anatomical image was collected (MPRAGE, 1 mm isotropic voxels, TR = 2000 ms, TE = 2.63 ms, FOV = 256 × 256 mm^2, 160 axial slices) with a 3-Tesla scanner (Siemens TIM Trio). MR-visible markers were placed at the fiducial points (nasion, left, and right pre-auricular points) to allow co-registration to the MEG coordinate system. T1 images were skull-stripped using AFNI's 3dSkullStrip function (Cox, 1996).

For stroke patients, lesion masks were produced with manual region of interest (ROI) drawing tools in AFNI, based on thresholded segmentation of the T1 image (FAST; Yang et al., 2001), as well as features of a co-registered T2-FLAIR image (see Kielar et al., 2016). A mask of the perilesional rim (10 mm radius surrounding the lesion) was generated by dilating the lesion mask by 10 voxels in all directions, and then taking the intersection with the grey matter segmentation image to exclude voxels outside the cortex.

To define anatomical regions of interest, the 116 ROI Automated Anatomical Labelling atlas (AAL; Tzourio-Mazoyer et al., 2002) was transformed to each participant's native anatomical space. First, ANTS (Avants et al., 2011) was used to compute a non-linear transform between the patient's T1-weighted structural image and a standard template brain in MNI space. Then, the inverse of this transform was used to warp the AAL atlas from MNI space to native anatomical space. Only the first 90 (non-cerebellar) ROIs were considered for further analysis.

2.3. MEG data collection

Resting-state MEG signals were acquired with a 151-channel CTF MEG system with axial-gradiometers (CTF, Coquitlam, Canada), with synthetic 3rd-order gradient noise reduction (Vrba and Robinson, 2001). Data was collected in a seated position for 5 min at 625 Hz (17 patients, 19 controls; Kielar et al., 2016) or 10 min at 1250 Hz (6 patients, 4 controls; Shah-Basak et al., 2020) while participants fixated on a white cross presented on a black background.

Head position within the dewar was measured at the beginning and end of the resting state acquisition with three coils placed at the fiducial points. Pre-acquisition to post-acquisition head movement was not found to differ between patients and controls in terms of total translation (patients median (SD) = 0.88 cm (1.3 cm), controls = 0.53 cm (1.11 cm), $U(N_{patient} = 23, N_{control} = 23) = 213$, $p = 0.131$) nor absolute rotation in the X axis (patients = 0.63° (1.80°), controls = 0.58° (0.62°), U = 251, $p = 0.388$), Y axis (patients = 0.58° (1.87°), controls = 0.51° (1.47°), U = 213, $p = 0.131$) or Z axis (patients = 0.46° (1.00°), controls = 0.39° (1.44°), U = 252, $p = 0.396$).

2.4. MEG preprocessing and source localization

Continuous MEG datasets were downsampled to 625 Hz (if recorded at 1250 Hz), band-pass filtered between 0.5 and 125 Hz, and divided into 5 s epochs. Bad channels and epochs contaminated by large artifacts were manually flagged and excluded from further analysis. An average of 60.9 epochs (SD = 8.7) were included for controls, and an average of 57.2 epochs (SD = 6.0) were included for the 17 patients from the Kielar et al. (2016) cohort. Due to the longer acquisition time, an average of 110.3 epochs (SD = 18.0) were included for the 6 patients from the Shah-Basak et al., (2020) cohort. For all patients and controls, the included number of epochs well exceeded recommendations for reliable estimation of periodic and aperiodic spectral parameters (Wiesman et al., 2022).

Synthetic Aperture Magnetometry (SAM; Vrba and Robinson, 2001) was used to localize signals to 90 virtual channels across the brain, each located at the center of an ROI. SAM is a scalar beamformer capable of estimating the time series of a spatially localized dipole as a weighted combination of the sensor time series. More specifically, SAM uses a head model and the covariance matrix of the sensor data to estimate a vector of sensor weights which act as a spatial filter, maximizing the power of a dipole at a given location while minimizing the influence of signals from other locations. In addition to providing source localization, this spatial filtering method also offers benefits in terms of noise reduction and rejection of artifacts originating from outside the brain volume (Cheyne et al., 2006, 2007; Kirsch et al., 2006).

To produce the head model, the T1-weighted anatomical image was transformed into the MEG coordinate system by aligning the MRI fiducial points with the average MEG head position (average of the head locator coil positions at the beginning and end of the acquisition). A 3D convex hull approximating the inner skull surface was generated from the anatomical image and used to produce a multi-sphere head model tangential to the hull surface (Huang et al., 1999).

Beamforming targets were generated by first transforming the AAL atlas to the MEG coordinate space using the same method as for the MNI space described above. Target spheres with a diameter of 10 voxels were then placed at the center of mass of each of the 90 non-cerebellar ROIs using AFNI (Cox, 1996). Any of the resulting target voxels that intersected with the lesion mask were excluded from beamforming. Any spheres that overlapped >50 % with the lesion itself were excluded from further analysis.

Finally, SAM was performed with CTF software (CTF; Port Coquitlam, British Columbia, Canada), computing covariance between 0 and 80 Hz, and generating a set of beamformer weights for each of the voxels belonging to the target spheres. To create a single summary time series for each ROI at each epoch, singular value decomposition (SVD) was computed on the matrix of beamformer weights associated with each sphere in MATLAB, and the first singular value was multiplied by the sensor time series for each epoch (Backus et al., 2016). The resulting time series was used to summarize the activity of the associated ROI for all subsequent analyses.

2.5. Frequency domain analysis

Specparam (Donoghue et al., 2020) employs an iterative model-fitting procedure to separately parameterize the aperiodic and periodic components of neural power spectra. The aperiodic component, reflecting neural dynamics without a characteristic frequency, is modelled as a straight line in log power vs log frequency coordinates. This line is parameterized by its slope (the aperiodic exponent) and an offset (y-intercept). In contrast, the periodic component captures an arbitrary number of narrowband peaks in the power spectrum associated with putative neural oscillations. After subtracting the aperiodic exponent, the peaks in the remaining periodic spectrum are fit with Gaussian functions in an iterative procedure, where each Gaussian is defined by center frequency, power, and bandwidth.

For each participant, *specparam* was applied to the average power spectral densities (PSDs) computed for each virtual channel. PSDs were computed on each epoch at all virtual channels using a smoothed FFT

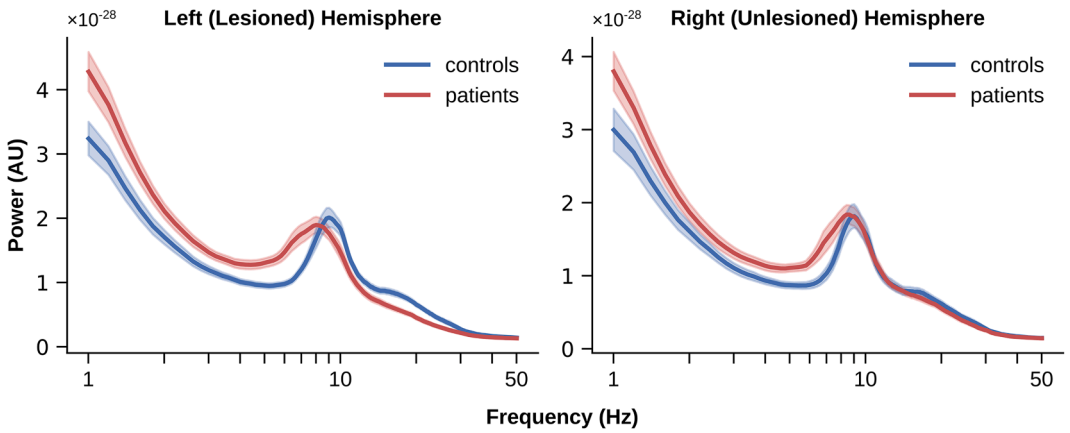

Fig. 1. Average power spectral densities (PSDs) for patients versus controls in the lesioned and unlesioned hemisphere. Shaded area represents standard error of the mean.

implemented in the *neurodsp* package in Python ('medfilt' option; Cole et al., 2019) and then averaged over epochs. *Specparam* model fitting was constrained between 1 and 50 Hz with no aperiodic knee, and a maximum of 4 peaks. PSDs averaged across each hemisphere are shown in Fig. 1 for patients and controls.

2.6. Time domain analysis

Since power in the frequency domain does not provide definitive evidence of a neural oscillation, lagged coherence (Fransen et al., 2015) was used as a complementary time-domain measure to quantify the periodic component. By quantifying rhythmicity in the time domain as the consistency of phase across time windows, lagged coherence provides stronger evidence for differences in genuinely periodic activity than spectral measures.

For each participant and ROI, lagged coherence was computed with *neurodsp* (Cole et al., 2019) on each epoch in 1 Hz increments from 1 to 50 Hz, using wavelets of three cycles in length, and the subsequent rhythmicity values were averaged across epochs.

3. Results

3.1. Spectral parameterization

Fig. 2 illustrates group averages of the estimated aperiodic fits and periodic spectra (power spectra after subtraction of the aperiodic fit).

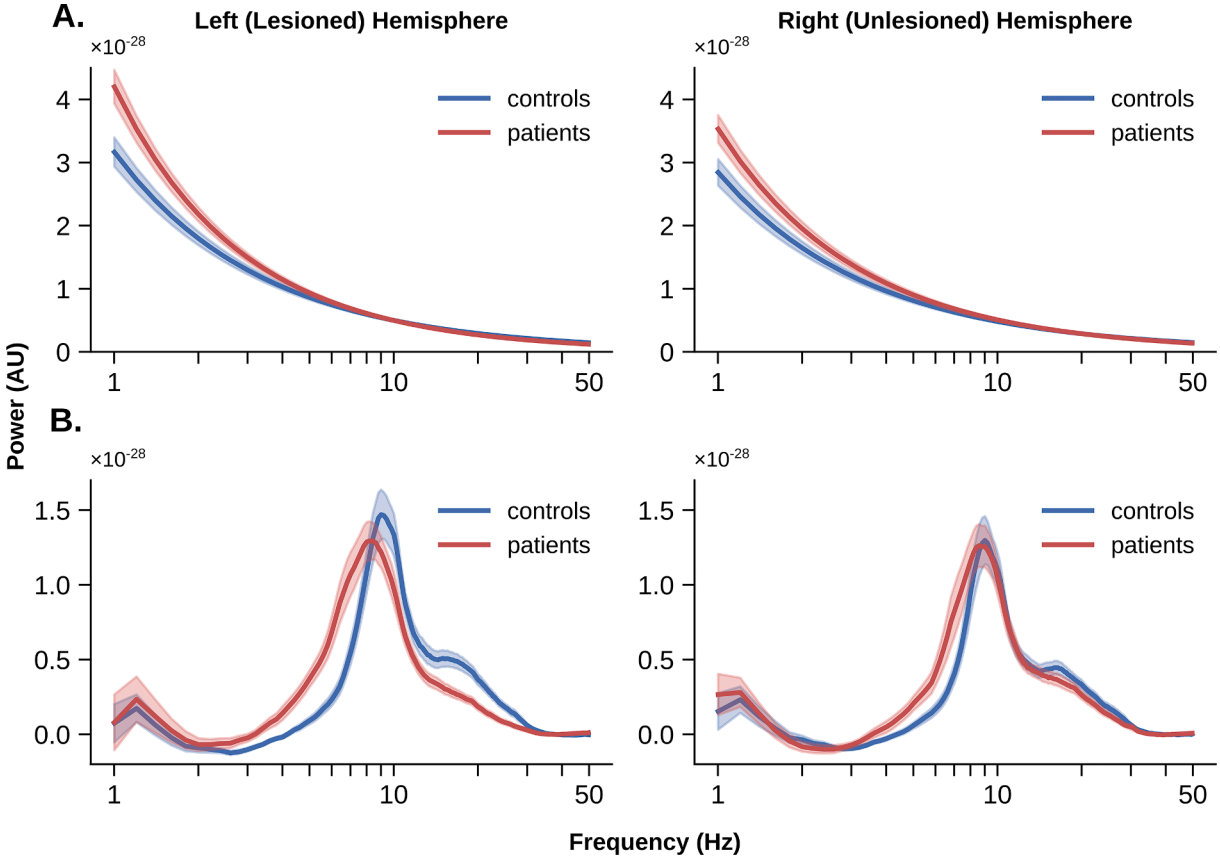

Fig. 2. A) Average aperiodic fits for patients versus controls in the lesioned and unlesioned hemisphere. B) Average periodic power spectra for patients versus controls in the lesioned and unlesioned hemisphere. Average periodic power spectra were computed by subtracting the aperiodic fit from the power spectrum at each ROI, then averaging across all ROIs within a hemisphere. Shaded areas represent standard error of the mean.

To parameterize the periodic component, representing the properties of putative oscillations, we examined the Gaussian functions fit to the peaks in the periodic power spectrum. Only two frequency bands reliably produced high power peaks across participants and virtual channels: 90 % of virtual channels had at least one peak identified within the range of 5–12 Hz (hereafter referred to as the theta-alpha range), and 88.7 % of virtual channels had at least one peak within the classical beta range (15–30 Hz). Together, these two ranges contained 83 % of all peaks identified in any band at any channel. Peaks were rarely identified within the classical delta band (1–4 Hz, 1.2 % of virtual channels) and gamma band (30–50 Hz; 12.4 % of all virtual channels). As such, only the theta-alpha and beta ranges could be adequately compared across participants, so only these ranges were considered. Specifically, we quantified the periodic component as the center frequency, power, and bandwidth of the tallest (highest power) peaks within the theta-alpha band and the beta band.

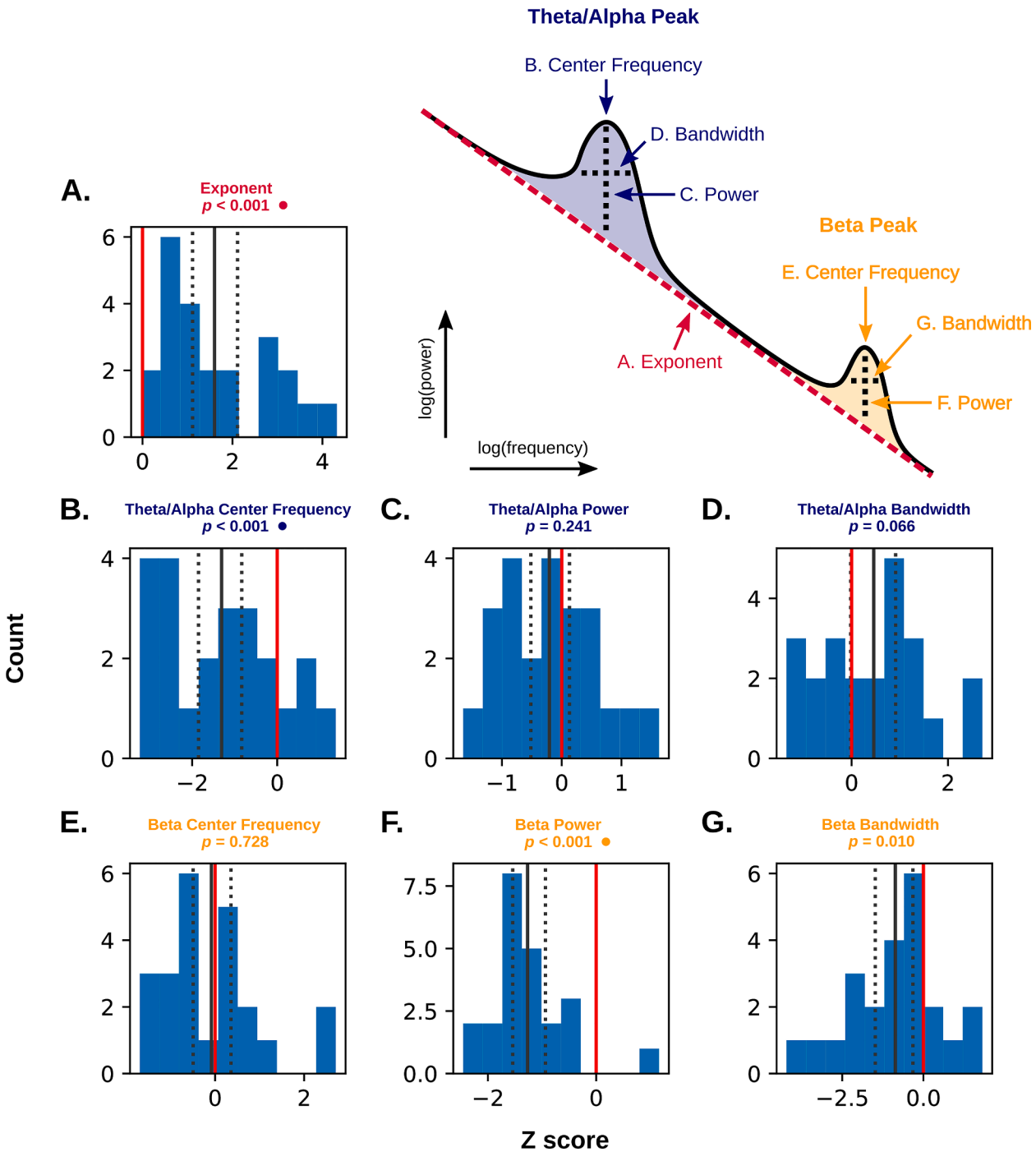

Fig. 3. Standardized differences (Z-scores) comparing average perilesional parameters in patients to individualized control distributions (see section 3.2) for the aperiodic component (A) and periodic component (B-G). Counts represent patients, with larger absolute values indicating greater deviation from controls (represented by the red line at zero). The solid black line represents the mean of the distribution, and dotted lines mark the upper and lower 95 % bootstrapped confidence limits (1000 resamples). P values marked with a circle are significant after Bonferroni correction (α (two-tailed) = 0.05/7 = 0.007). Upper right: idealized neural power spectrum illustrating the seven spectral parameters under investigation. (For interpretation of the references to colour in this figure legend, the reader is referred to the web version of this article.)

Table 2
Comparing perilesional dynamics with equivalent areas in controls. Parameters in bold are significantly different at perilesional ROIs compared to corresponding ROIs from control participants at α = 0.05 (two-tailed). Parameters with an asterisk are significantly different after Bonferroni correction (frequency domain α = 0.05/7 = 0.007, time domain α = 0.05/3 = 0.017). 'Mean' refers to the average value of the given parameter for perilesional ROIs in patients, while 'Mean standardized difference from controls' refers to the average, standardized difference (Z-score) between patients and their individualized control distributions (see section 3.2). EXP = aperiodic exponent, TACF/TAPW/TABW = theta-alpha center frequency/power/bandwidth, BCF/BPW/BBW = beta center frequency/power/bandwidth, DLC/TALC/BLC = delta/theta-alpha/beta lagged coherence.

	Parameter	Mean (SD)	Mean standardized difference from controls (SD)	*t(22)*	*p*
Frequency domain	**EXP***	0.92 (0.12)	1.60 (1.20)	6.25	<0.001
	TACF*	8.38 (0.88)	−1.31 (1.29)	−4.76	<0.001
	TAPW	0.58 (0.15)	−0.21 (0.80)	−1.21	0.24
	TABW	3.02 (0.57)	0.46 (1.12)	1.94	0.07
	BCF	18.77 (2.10)	−0.08 (1.10)	−0.36	0.73
	BPW*	0.26 (0.10)	−1.27 (0.71)	−8.37	<0.001
	BBW	6.16 (2.15)	−0.87 (1.44)	−2.83	0.01
Time domain	DLC	0.69 (0.01)	−0.23 (1.45)	−0.74	0.46
	TALC	0.27 (0.01)	−0.19 (0.64)	−1.39	0.18
	BLC*	0.16 (0.01)	−0.85 (0.66)	−6.04	<0.001

The aperiodic component, representing the scaling of the 1/f background, is parameterized by an exponent (slope) and offset (y-intercept). Only the exponent was considered, as the offset was found to be highly redundant across patients and controls (r = 0.86), suggesting that variation in the offset (y-intercept) was largely driven by variation in the spectral slope rather than uniform changes in power across frequencies.

In summary, power spectra were quantified with seven parameters: aperiodic exponent (EXP), theta-alpha center frequency, power, and bandwidth (TACF, TAPW, and TABW), and beta center frequency, power, and bandwidth (BCF, BPW, and BBW; see Fig. 3, upper right). To align time domain parameters with these definitions, band-specific lagged coherence (LC) estimates were computed by averaging over the delta (DLC; 1–4 Hz), theta-alpha (TALC; 5–12 Hz) and beta (BLC; 15–30 Hz) frequency ranges.

3.2. Perilesional abnormalities

To investigate abnormalities in tissue close to the lesion, a small group of perilesional ROIs were identified for each patient and compared to controls. Without acute perfusion data, the tissue plausibly disrupted by hypoperfusion (but not fully infarcted) can only be determined heuristically. We therefore considered any ROI that had at least 10 % of its volume within 10 mm of the lesion as 'perilesional' (mean number of ROIs included = 12.9, SD = 5.5, range = 5–23), and signal features derived from their central spheres were included in subsequent analyses.

Abnormalities within these perilesional ROIs were then assessed by comparing each patient to a unique control distribution reflecting their individual perilesional anatomy. For each patient, spectral parameters and lagged coherence values were first averaged over all perilesional ROIs. These values were then standardized based on the distribution resulting from averaging over the same subset of ROIs for each control participant. As such, the resulting Z-score indexes deviation from the individualized control distribution mean. Group differences in each parameter were therefore assessed by comparing these Z-scores to a value of 0 (representing no difference between patients and controls) using a single sample *t*-test (Table 2; two-tailed with Bonferroni correction, frequency domain α = 0.05/7 = 0.007, time domain α = 0.05/3 = 0.017; *scipy.stats*, Virtanen et al., 2020).

In the frequency domain, three spectral parameters were found to differ significantly between patients and controls after Bonferroni correction for multiple comparisons (Fig. 3). Namely, perilesional tissue exhibited a higher aperiodic exponent (steeper slope), lower theta-alpha center frequency, and lower beta power. *Specparam* fit error did not differ significantly between perilesional ROIs and comparable ROIs in controls (mean standardized difference from controls = 0.035 (0.006), t(22) = 1.343, *p* = 0.193).

In the time domain, lagged coherence revealed differences in the

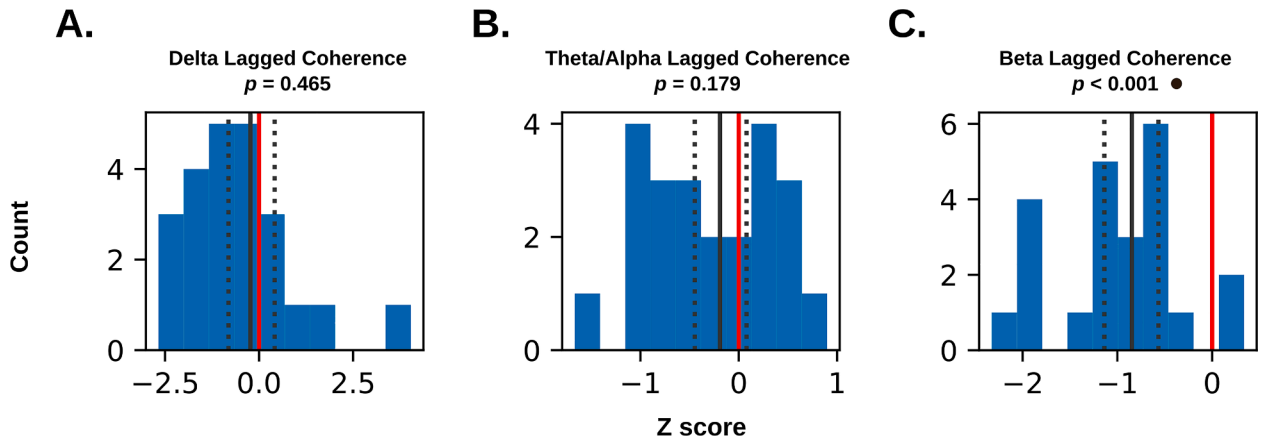

Fig. 4. Standardized differences (Z-scores) comparing average perilesional lagged coherence in patients to individualized control distributions (see section 3.2). Counts represent patients, with larger absolute values representing greater deviation from controls (represented by the red line at zero). The solid black line represents the mean of the distribution, and dotted lines mark the upper and lower 95 % bootstrapped confidence limits (1000 resamples). P values marked with a circle are significant after Bonferroni correction (α (two-tailed) = 0.05/3 = 0.017). (For interpretation of the references to colour in this figure legend, the reader is referred to the web version of this article.)

beta band only, with perilesional tissue exhibiting lower beta rhythmicity compared to the same regions in controls (Fig. 4). Contrary to the typical interpretation of elevated low frequency oscillations in stroke, perilesional tissue did not exhibit significantly elevated rhythmicity in the delta or theta-alpha bands. Narrow bootstrapped 95 % confidence intervals overlapping with zero (Fig. 4A-B) suggest the absence of a significant difference in delta/theta-alpha is more consistent with a lack of group differences, rather than high error variance.

It should be noted that both *specparam* and lagged coherence are susceptible to biases related to changes in the aperiodic exponent, and *specparam* may also be biased by the presence of a high amplitude oscillation at the lower edge of the fitting range (Gerster et al., 2021). See Appendix A for simulations demonstrating that these effects are unlikely to be responsible for the results observed here.

Finally, we considered whether abnormalities in any perilesional features covaried with the amount of time elapsed since stroke, potentially suggesting long term changes in perilesional electrophysiological dynamics across the chronic phase of the disease. Except in the case of beta power (Pearson $r = 0.508$, $p = 0.013$), time elapsed since stroke did not relate significantly to deviation in frequency domain nor time domain features relative to controls ($|\text{Pearson r}| = 0.060–0.339$, $p = 0.117–0.787$), and no relationships survived Bonferroni correction for multiple comparisons.

3.3. Identifying abnormalities beyond the perilesional area

Given the highly interconnected nature of the brain, it is expected that a focal lesion should produce abnormal dynamics more broadly throughout the brain ('diaschisis'). To account for the heterogeneity in lesion size and location, two different approaches were taken to explore these more distributed effects. First, parameters were averaged over the entire un-lesioned (right) hemisphere and compared to the lesioned (left) hemisphere, as well as left and right hemispheres in controls. Considering each hemisphere as a whole provides a simple means of detecting broad differences in the un-lesioned hemisphere, irrespective of any variation caused by individual differences in lesion size and location. Each averaged parameter was submitted to Tukey's HSD (Wilkinson, 1999; Lane, 2010) to assess pairwise differences between hemispheres (Table 3; two-tailed with Bonferroni correction, frequency domain $\alpha = 0.05/7 = 0.007$, time domain $\alpha = 0.05/3 = 0.017$; *scipy.stats*, Virtanen et al., 2020).

The un-lesioned (right) hemisphere showed a significantly higher aperiodic exponent compared to controls ($p = 0.011$), but significantly lower than the lesioned (left) hemisphere ($p = 0.032$; Fig. 5), however these differences did not survive Bonferroni correction. Mean theta-alpha frequency and beta power were also both decreased in the un-lesioned hemisphere, however they were not significantly different from either the lesioned hemisphere or the healthy right hemisphere in controls, suggesting that they may be intermediate between the lesioned and healthy control hemispheres. As expected, the lesioned (left) hemisphere demonstrated a significantly higher aperiodic exponent, lower theta-alpha center frequency (at $\alpha = 0.05$ only), and lower beta power compared to both left and right hemispheres in controls, reproducing the pattern of effects seen in the perilesional ROIs above. There were no significant differences in *specparam* fit error between any pair of hemispheres ($0.74 < p < 0.9$ for all comparisons).

Table 3
Tukey's HSD results comparing hemisphere-average parameters between patients and controls. Parameters in bold show significant pairwise differences (row vs column) at $\alpha < 0.05$ (two-tailed). Parameters with an asterisk are significantly different after Bonferroni correction (frequency domain $\alpha = 0.05/7 = 0.007$, time domain $\alpha = 0.05/3 = 0.017$). EXP = aperiodic exponent, TACF/TAPW/TABW = theta-alpha center frequency/power/bandwidth, BCF/BPW/BBW = beta center frequency/power/bandwidth, DLC/TALC/BLC = delta/theta-alpha/beta lagged coherence.

Patient R (Un-lesioned)		diff	p-adj
	EXP	**0.079**	**0.032**
	TACF	-0.411	0.36
	TAPW	-0.016	0.9
	TABW	0.049	0.9
	BCF	-0.272	0.9
	BPW	-0.041	0.454
	BBW	-0.029	0.9
	DLC	-0.001	0.9
	TALC	-0.001	0.9
	BLC	**-0.003**	**0.019**

Control L		diff	p-adj	EXP	diff	p-adj
	EXP*	**0.122**	**0.001**	TACF	0.043	0.308
	TACF	**-0.743**	**0.020**	TAPW	-0.332	0.543
	TAPW	-0.038	0.828	TABW	-0.022	0.9
	TABW	0.258	0.167	BCF	0.210	0.334
	BCF	-0.016	0.9	BPW	0.256	0.9
	BPW*	**-0.111**	**0.001**	BBW	-0.070	0.065
	BBW	-0.729	0.226	DLC	-0.700	0.259
	DLC	-0.001	0.9	TALC	0.001	0.9
	TALC	-0.002	0.836	BLC	-0.001	0.9
	BLC*	**-0.004**	**0.002**	EXP	-0.001	0.833

Control R		diff	p-adj		diff	p-adj		diff	p-adj
	EXP*	**0.155**	**0.001**	**EXP**	**0.076**	**0.011**	EXP	0.032	0.559
	TACF	**-0.786**	**0.012**	TACF	-0.375	0.445	TACF	-0.043	0.9
	TAPW	-0.016	0.9	TAPW	-0.001	0.9	TAPW	0.022	0.9
	TABW	0.321	0.054	TABW	0.272	0.132	TABW	0.063	0.9
	BCF	-0.087	0.9	BCF	0.185	0.9	BCF	-0.071	0.9
	BPW*	**-0.095**	**0.006**	BPW	-0.053	0.229	BPW	0.017	0.9
	BBW	-0.487	0.566	BBW	-0.458	0.608	BBW	0.242	0.9
	DLC	0.001	0.9	DLC	0.001	0.841	DLC	0.001	0.867
	TALC	-0.002	0.710	TALC	-0.001	0.9	TALC	-0.001	0.9
	BLC	**-0.003**	**0.030**	BLC	0.001	0.9	BLC	0.001	0.740
	Patient L (Lesioned)			**Patient R (Un-lesioned)**			**Control L**		

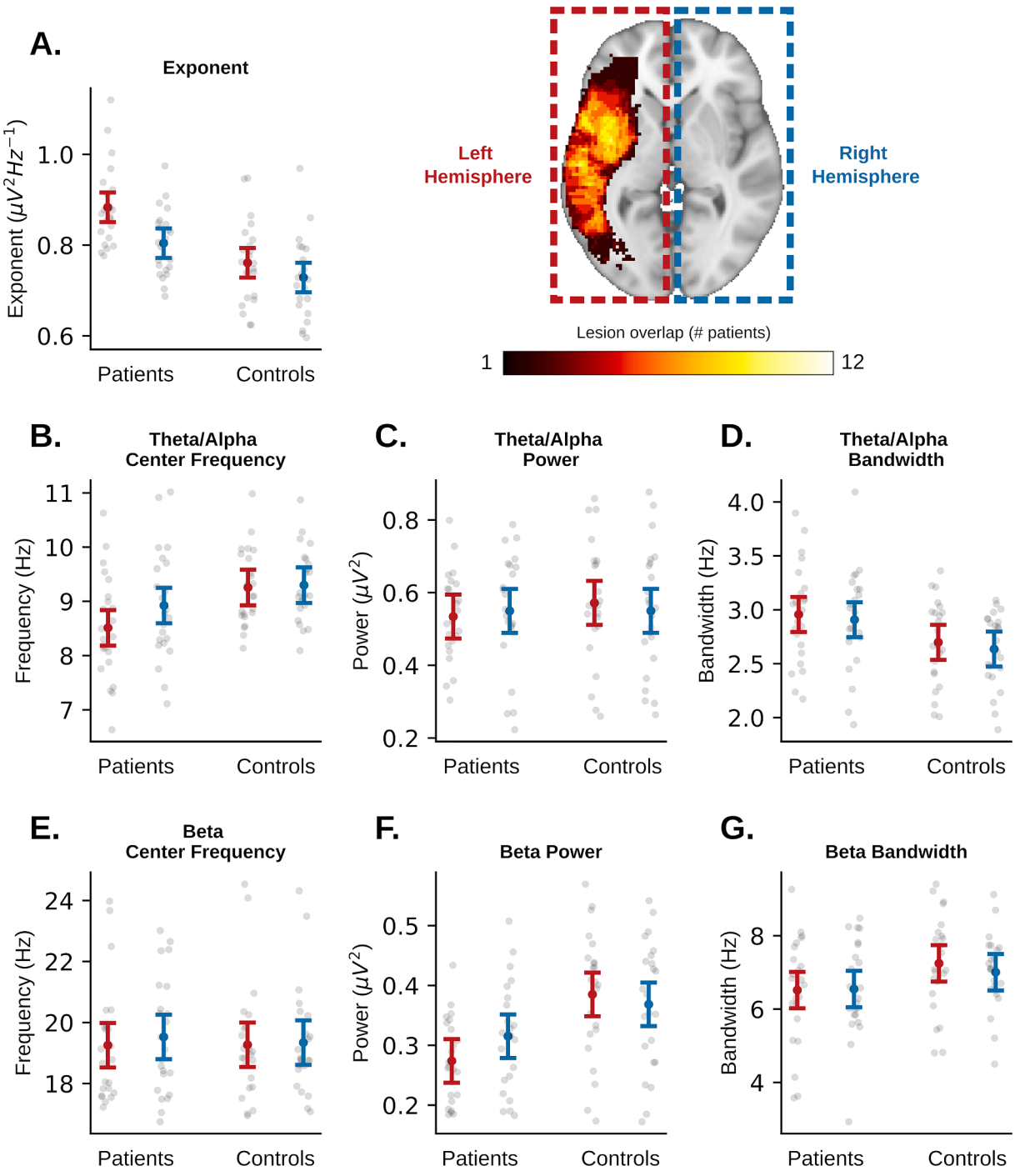

Fig. 5. Comparing hemisphere-average aperiodic (A) and periodic (B-G) parameters between patients and controls. Whiskers represent a universal confidence interval computed from Tukey's Q critical value (Hochberg and Tamhane, 1987; Seabold and Perktold, 2010).

In the time domain, the un-lesioned hemisphere showed no significant differences in delta, theta-alpha, or beta rhythmicity compared to controls (Fig. 6). As above, the lesioned left hemisphere showed significantly lower beta rhythmicity compared to controls and the un-lesioned right hemisphere, but only the comparison between lesioned hemisphere and left control hemisphere survived Bonferroni correction.

As a complementary approach, Partial Least Squares (PLS; McIntosh and Lobaugh, 2004) was used to visualize which ROIs most reliably demonstrate abnormalities in patients. PLS is a multivariate statistical technique that extracts patterns that maximally distinguish two groups, in this case patients and controls. PLS was computed on a brain data matrix containing EXP, TACF, and BPW for each participant and virtual channel. Since PLS requires an equal number of observations for every participant, any ROI that was too damaged by the lesion to be included for one patient (>50 % of the MEG sphere target overlapped with the lesion mask) had to be excluded for all participants. This left 69 ROIs in total: 14 in the left hemisphere and 45 in the right. Additionally, a small number of ROIs had no peaks detected in either the theta-alpha or beta bands for some participants, so these were filled with *missmda,* an imputation method based on principal components analysis (PCA; Josse et al., 2011). 6.5 % of the patient input data and 4.6 % of the control data was imputed.

The resulting latent variable (LV; $p = 0.034$, singular value = 3.068) was used to visualize differences between patients and controls. Fig. 7

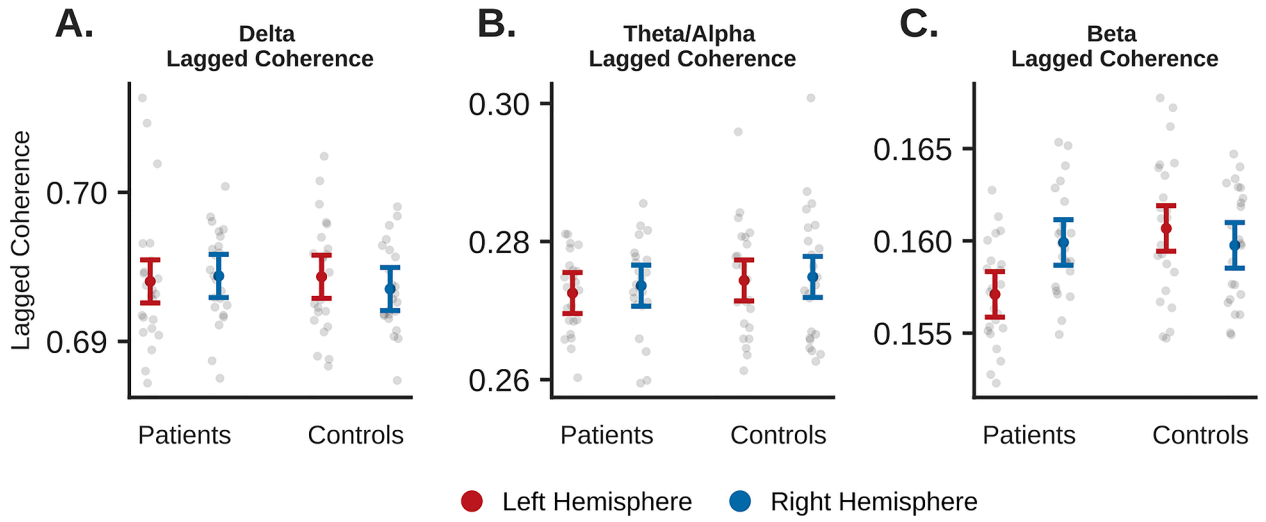

Fig. 6. Comparing hemisphere-average lagged coherence between patients and controls. Whiskers represent a universal confidence interval computed from Tukey's Q critical value (Seabold and Perktold, 2010; Hochberg and Tamhane, 1987).

displays the spatial distribution of bootstrap ratios (a measure of reliability) captured by LV1 for each parameter relative to the spatial distribution of lesions across participants.

3.4. Exploring dependencies between parameters

Having identified three ways that neural dynamics differ in chronic stroke, the question remains whether these abnormal features are related. To explore this, we used PCA to investigate patterns of covariation among the frequency domain features (*scikit-learn,* Pedregosa et al., 2011). More specifically, we examined how deviation from putatively normal values for a given feature at a given ROI (defined as the mean of the control group) was associated with deviation in the other parameters. To this end, we standardized all parameter values at each ROI individually based on the mean and SD of the control group at that ROI. We then computed PCA on the standardized control and patient data separately, treating each ROI for each participant as an individual observation (input matrix: ROIs * participants × spectral parameters).

Fig. 8A depicts the loadings of the first two principal components (PCs). In both cases extremely similar components were extracted for both patients and controls (cosine similarity for PC1 = 0.96, PC2 = 0.89). The implications of this similarity are addressed in the Discussion. PC1 accounted for 24 % of total variability in patients and 21 % in controls, while PC2 accounted for 20 % of total variability in patients and 21 % in controls.

Notably, PC2 seemed to capture the "slowing" observed in patients. More specifically, it showed a negative relationship between aperiodic exponent and theta-alpha center frequency as well as beta power, reflecting the pattern observed in both the perilesional and whole brain analyses. If this is the case, we expected a negative relationship between PC2 score and distance to the lesion (defined here as Euclidean distance from the center of the ROI sphere to the nearest voxel in the lesion mask). To investigate this, we fit a linear mixed effects model over all ROIs in the lesioned hemisphere, with either PC1 or PC2 as the dependent variable (Table 4). The model estimated the fixed between- and within-patient effects, respectively, by including the patient-average distance to lesion and mean-centered distance to lesion as predictors. Random slope and intercept were estimated for the within-subjects effect to quantify inter-patient variability. Models were fit with the *lme4* package in R (Bates et al., 2015; $\alpha = 0.05$, two-tailed). As predicted, PC2 demonstrated a significant negative relationship with mean-centered distance to lesion ($\beta = -0.022$, $p < 0.001$; Fig. 8C), while PC1 did not ($\beta = -0.004$, $p = 0.233$; Fig. 8B). Neither PC demonstrated a significant between patients effect.

We also considered whether biases inherent to the *specparam* algorithm itself may be responsible for the dependencies observed between the estimated spectral parameters. To investigate, we applied *specparam* on simulated power spectra with no correlations among their spectral features (see Appendix B). PCA on the subsequent parameter estimates produced a first principal component similar to PC1 (cosine similarity with patient PC1 = 0.67; control PC1 = 0.72), but less similar to PC2 (cosine similarity with patient PC2 = 0.34; control PC2 = 0.27), suggesting PC1 may represent dependencies imparted by *specparam*, rather than those of biological origin.

3.5. Linking abnormal neural dynamics to neurocognitive outcomes

Finally, we considered how abnormal neural dynamics related to cognitive impairment in seventeen patients with neurocognitive assessment data (Kielar et al., 2016). Following previous work using a similar assessment (Shah-Basak et al., 2018), we focused on three groups of tests assessing language, memory, and executive function.[1] We predicted that the slowing pattern observed above, reflected in either the individual spectral parameters (EXP, TACF, and BPW) or the multivariate "slowing" component (PC2), would covary with the severity of cognitive impairment.

To quantify cognitive function in the three cognitive domains, each measure was standardized by its mean and standard deviation within the sample, and the resulting Z-scores were averaged within each domain. We then employed Behaviour PLS (McIntosh and Lobaugh, 2004) to identify patterns of maximal covariation between the brain data matrix (average spectral parameters or PC2 values) and the behavioural data (average language, memory, and executive functioning scores).

[1] Language: Western Aphasia Battery (Kertesz, 1982), Northwestern Assessment of Verbs and Sentences VNT/VCT/SCT/SPT (Cho-Reyes and Thompson, 2012), Aphasiabank Sentence Repetition (Macwhinney et al., 2011), Boston Naming Test (Kaplan et al., 2001), Peabody Picture Vocabulary Test (Dunn and Dunn, 1997). Memory: Kaplan Baycrest Neurocognitive Assessment (KBNA; Leach et al., 2000) complex figure drawing (immediate recall/delayed recall/delayed recognition) and word lists (immediate recall/delayed recognition), Wechsler Memory Scale-IV logical memory (immediate recall/delayed recall/delayed recognition). Executive Function: Wechsler Adult Intelligence Scale-IV digit span (forward/backward), Delis-Kaplan executive function system (D-KEFS; Delis et al., 2001) trails making test (TMT-A/TMT-B), KBNA symbol cancellation (Leach et al., 2000).

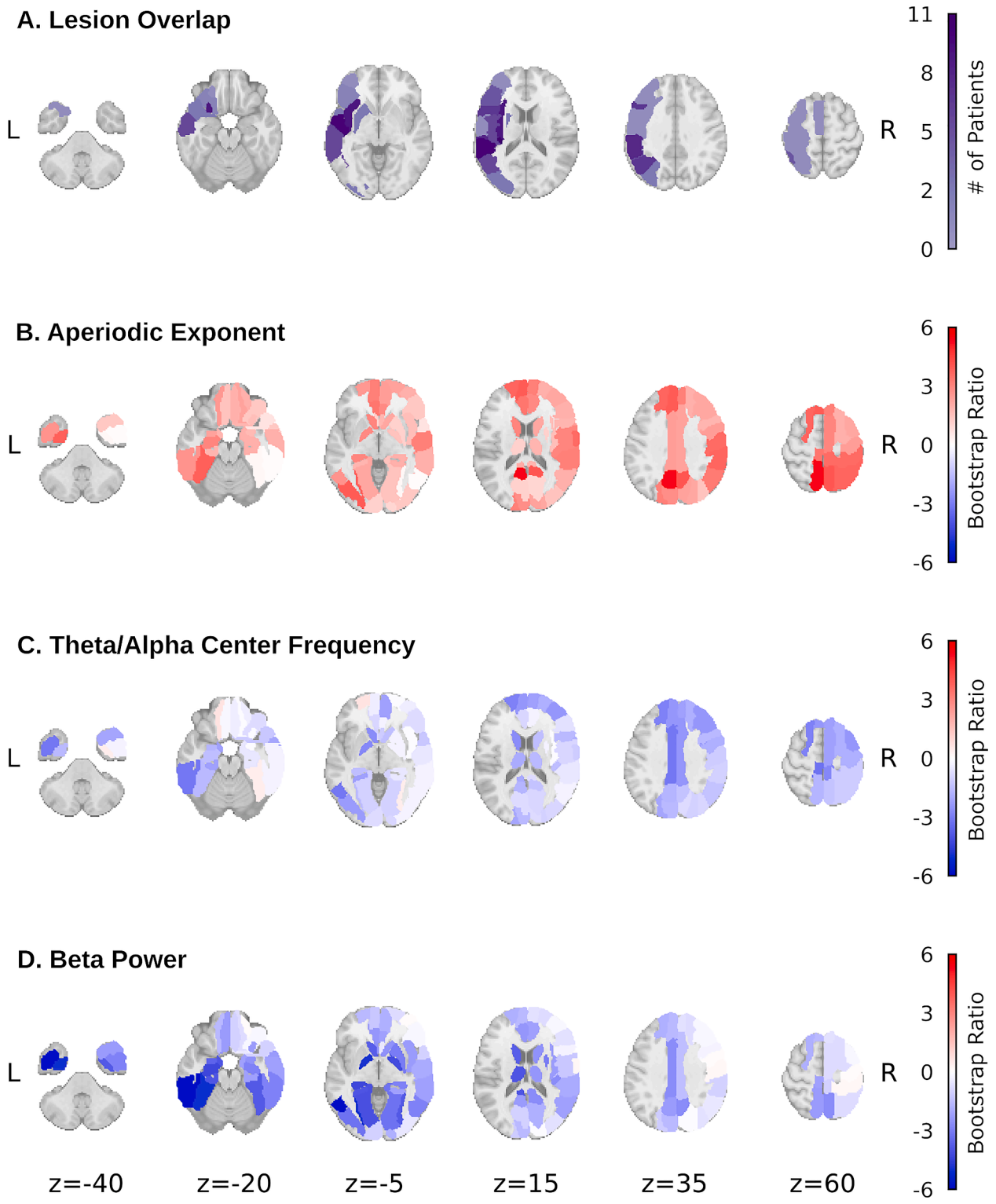

Fig. 7. LV1 bootstrap ratios for the three spectral parameters of interest (B-D), with region-wise overlap in lesion presence across patients provided for comparison (A). Absolute values of the bootstrap ratios reflect reliability of group differences at each ROI as determined by bootstrap resampling (1000 permutations; McIntosh and Lobaugh, 2004). Positive values indicate higher parameter values for patients, negative values indicate higher values for controls.

Statistical inference was determined with permutation testing (1000 iterations) with a significance threshold of $p < 0.05$ (two-tailed).

As with previous analyses, we considered the effect of both localized (perilesional) and distributed abnormalities on cognitive impairment. To investigate the former, the three abnormal parameters identified previously (EXP, TACF, and BPW) were averaged across perilesional ROIs for each patient. PLS relating the resulting brain matrix to the behavioural matrix extracted three LVs (singular values = 0.91, 0.27, and 0.11), and only the first passed the significance threshold ($p = 0.046$). This LV showed the predicted pattern, with brain data saliences (analogous to factor/component loadings) reflective of slowing (EXP = 0.69, TACF = −0.23, BPW = −0.69) relating to negative behaviour

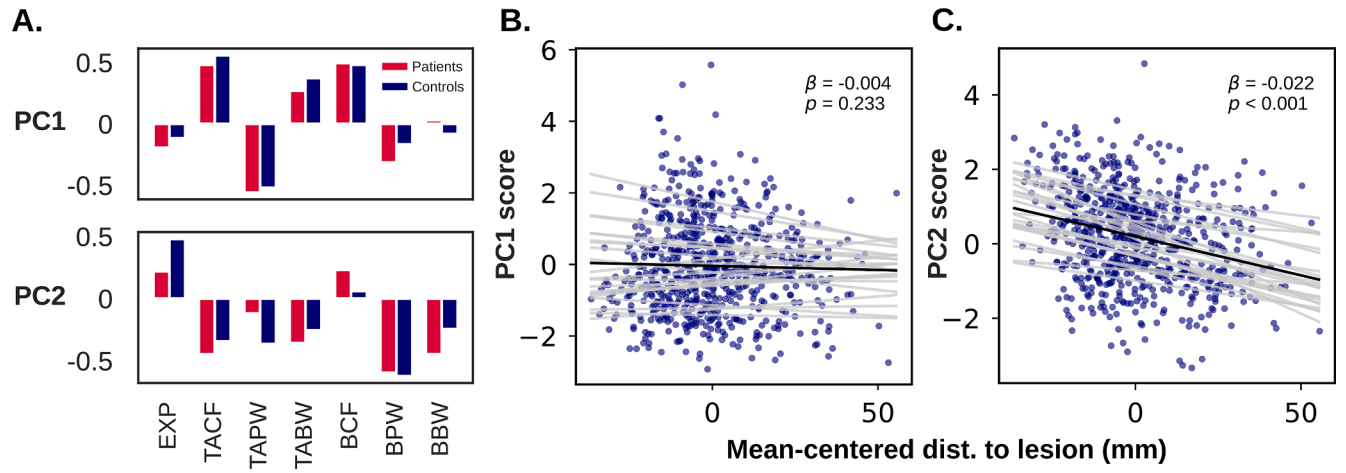

Fig. 8. A) The first two principal components (PCs) extracted from the standardized spectral parameter scores in patients and controls. B and C) Relationship between PC scores and mean-centered distance to lesion (Euclidean distance to nearest lesioned voxel minus patient mean). Grey lines represent the random intercept and slope estimated for each patient. EXP = aperiodic exponent, TACF/TAPW/TABW = theta-alpha center frequency/power/bandwidth, BCF/BPW/BBW = beta center frequency/power/bandwidth.

Table 4
Linear mixed effects model results reflecting the relationship between spectral parameter principal components (PC1 or PC2) and distance from the lesion. The model estimated the fixed between- and within-patient effects, respectively, by including the patient-average distance to lesion and mean-centered distance to lesion as predictors. Random slope and intercept were estimated for the within-subjects effect to quantify inter-patient variability.

PC1	**Fixed Effect**	**Estimate (SE)**	**t**	***p***
	Intercept	0.392 (0.520)	0.753	0.451
	Within patient	−0.004 (0.003)	−0.795	0.233
	Between patients	−0.015 (0.019)	−1.193	0.427
	Random Effect (within patient)	**Variance (SD)**		
	Intercept	0.795 (0.892)		
	Slope	<0.001 (0.011)		
PC2	**Fixed Effect**	**Estimate (SE)**	**t**	***p***
	Intercept	0.299 (0.457)	0.655	0.512
	Within patient*	−0.022 (0.004)	−6.014	<0.001
	Between patients	0.001 (0.017)	0.057	0.955
	Random Effect (within patient)	**Variance (SD)**		
	Intercept	0.527 (0.726)		
	Slope	<0.001 (0.012)		

saliences in all three cognitive domains (Language = −0.40, Memory = −0.84, Executive = −0.37), indicating that greater slowing was associated with more severe cognitive impairment. The same approach with the multivariate slowing component (PC2) derived previously yielded a first LV (singular value = 0.58) with a similar pattern of behavioural saliences (Language = −0.32, Memory = −0.91, Executive = −0.25), but which did not pass the significance threshold ($p = 0.145$). Similarly, averaging within the left and right hemispheres to consider the impact of broader abnormalities showed similar patterns for the three spectral parameters (singular value = 0.8, $p = 0.331$) and PC2 (singular value = 0.66, $p = 0.135$), but did not pass the significance threshold. No significant LVs relating PC1 and cognitive scores were found when averaging within perilesional ROIs (singular value = 0.210, $p = 0.863$), or hemispheres (singular value = 0.391, $p = 0.341$).

4. Discussion

4.1. Aperiodic abnormalities

With a combination of frequency and time domain measures, we have demonstrated that both periodic and aperiodic dynamics are disrupted in chronic stroke. Contrary to typical interpretations, the most readily detectable difference between patients and controls is steepening of the aperiodic power spectrum in patients, not an enhancement of low frequency periodic activity. The latter was unsupported due to a lack of enhanced delta rhythmicity, and lack of delta peaks in the aperiodic-corrected spectrum. This mirrors findings in rats after middle cerebral artery occlusion, where acutely increased EEG spectral slope was associated with poorer motor function, and slow wave activity (assessed in the time domain) was not found to be related to this effect (Leemburg et al., 2018).

Overall, these results suggest a need to reinterpret the existing electrophysiological literature in stroke, with new emphasis on the implications of the steeper aperiodic background, rather than low frequency oscillations. A steeper aperiodic slope reflects greater autocorrelation in the time domain, such that successive electrophysiological measurements are more highly correlated with each other, and remain correlated over longer temporal intervals. This phenomenon has been associated with the effects of anesthesia (Colombo et al., 2019) and sleep (Freeman and Zhai, 2009; Lendner et al., 2020). The opposite effect is seen in the waking state during task performance, where spectral slopes flatten as task demands increase (He, 2014; Podvalny et al., 2015), suggesting more efficient information processing (He, 2011). As such, the chronically steepened aperiodic spectra observed here may reflect a reduction in complexity (Sarasso et al., 2020; Zappasodi et al., 2014) and diminished capacity for information processing in affected tissue, potentially explaining its association with cognitive impairment.

The underlying causes of aperiodic scaling in electrophysiological spectra are still debated, as many generative mechanisms are capable of producing power-law behavior (He et al., 2010). However, attention has turned recently to the balance of excitation and inhibition (E:I ratio) – a property known to be disrupted in stroke (Carmichael, 2016). Both computational (Chini et al., 2021; Gao et al., 2017; Lombardi et al., 2017; Rowe et al., 2004; Trakoshis et al., 2020) and experimental evidence (Chini et al., 2021; Gao et al., 2017; Trakoshis et al., 2020; Waschke et al., 2021) have identified E:I ratio as a potential determinant of spectral slope, with most of these authors concluding that a decrease in the E:I ratio (increase in inhibition relative to excitation) produces a steeper slope. In stroke, increased tonic GABAergic inhibition has indeed been observed after experimentally-induced lesions in mice (Clarkson et al., 2010; Orfila et al., 2019). However, some computational models demonstrate the opposite pattern, with higher E:I ratio (increased excitation relative to inhibition) producing steeper spectral slopes (Lombardi et al., 2017; Rowe et al., 2004). Similarly, some clinical data

suggests that stroke patients may in fact have a deficit in inhibition, including a selective loss of GABAergic receptors (Chida et al., 2011; Dong et al., 1997), with sporadic case reports of dramatic improvements in clinical function in response to GABAergic agonists (Cohen et al., 2004; Hall et al., 2010). More data will be necessary to resolve the directionality linking E:I ratio to spectral slope.

If indeed spectral abnormalities are ultimately explainable as alterations of E:I balance, normalizing these dynamics and rehabilitating affected tissue may be possible with neuromodulation of excitability. Alternatively, there remains the possibility that structural damage disrupting coordination between brain regions could be responsible for the steepening of the aperiodic slope. For instance, disruption of thalamocortical connections via white matter lesions has been associated with increased power in the delta band and suppression of fast activity (Kaplan and Rossetti, 2011) – an effect which may in fact reflect a rotation of the aperiodic power spectrum, as demonstrated here.

4.2. Periodic abnormalities

In addition to substantial difference in the aperiodic component, stroke patients also exhibited differences in putative oscillatory activity. First, stroke patients showed slowing of the peak alpha frequency after correcting for the aperiodic slope, corroborating previous reports of the same (Giaquinto et al., 1994; Jordan, 2004; Juhasz and Kamondi, 1997; Tecchio et al., 2005; van Wijngaarden et al., 2016). When measuring power in the classical frequency bands, this slowing could have previously been interpreted as a power decrease in the alpha band (e.g. Machado et al., 2004; Nagata et al., 1989), and further contributed to differences in the ratio of lower to higher frequencies used in clinical prognosis (Finnigan and van Putten, 2013).

To the extent that alpha rhythm generation relies on corticothalamic interactions (Lopes da Silva et al., 1980; Steriade et al., 1990), stroke could disrupt alpha rhythms by damaging these connections. Indeed, disorders characterized by white matter lesions, such as vascular dementia (Moretti, 2004; Neto et al., 2015; Signorino et al., 1995) and multiple sclerosis (Kim et al., 2019) also demonstrate alpha slowing, while tumors of the white matter have also been associated with alpha slowing (Gloor et al., 1968). Unlike aperiodic steepening, it is unclear how E:I balance could affect alpha frequency. As such, disruption of corticothalamic connections should still be considered as a possible cause unifying both aperiodic steepening and alpha slowing.

Finally, converging results from frequency and time domain measures here indicate that stroke-related decreases in beta power (Jordan, 2004; Kielar et al., 2016; Shah-Basak et al., 2020; Tecchio et al., 2005; van Wijngaarden et al., 2016; Wu et al., 2016) are not just due to the steepening of the aperiodic slope, but rather the suppression of rhythmic activity in the beta band. Beta oscillations, classically considered a sensorimotor rhythm (but also detectable in non-sensorimotor areas; Law et al., 2022) appear to be broadly associated with endogenous "top-down" controlled processing (Engel and Fries, 2010; Spitzer and Haegens, 2017). Given that beta oscillations are known to occur in bursts (Jones, 2016; Law et al., 2022), decreased beta power could therefore also reflect fewer, shorter, or lower amplitude beta bursts. Since beta activity is also thought to be generated by thalamocortical interactions (Law et al., 2022) and is sensitive to E:I balance (Rossiter et al., 2014), stroke could plausibly disrupt beta activity through either or both of these routes, as described above. Future work considering both E:I balance and thalamocortical interactions will be needed to clarify these relationships.

4.3. Dependencies between parameters

Multivariate analysis identified dependencies between spectral parameters, suggesting that deviations in these spectral parameters could share a common cause. While PC1 may have been an artifact of spectral parameterization (Appendix B), PC2 appeared to capture the same pattern of stroke-related electrophysiological abnormalities identified in the univariate analyses, and correlated with proximity to the lesion. As such, PC2 may capture an electrophysiological pattern indicating stroke-related dysfunction, capturing the various facets of "spectral slowing" as described across the literature.

Intriguingly, both PC1 and PC2 were identified in controls as well as patients. This indicates that the same dependencies exist between spectral parameters in both healthy brains and brains afflicted with chronic stroke, suggesting that the abnormalities in stroke reflect a quantitative rather than qualitative change. In other words, stroke may cause electrophysiological dynamics to deviate away from normal, but the patterns of covariation among spectral features remain the same, even at these extremes. This remains speculative, however, and further investigation of the dependencies between spectral features (both physiological and artefactual) is needed.

4.4. Distributed abnormalities

Abnormal electrophysiological dynamics were detected in the unlesioned hemisphere, albeit weakly, suggesting the presence of diaschisis. Qualitatively, these dynamics appeared to deviate from controls in the same way as the lesioned hemisphere, although to a lesser degree. This raises questions about how a focal lesion can produce qualitatively similar disruption across widely distributed tissue, namely whether the stroke event causes widespread cellular changes (e.g. abnormal receptor expression or neurotransmitter reuptake), or rather abnormal dynamics propagate from the perilesional area throughout connected brain networks.

4.5. Limitations and future directions

Stroke patients are a diverse group, and our sample was relatively homogenous, comprising only chronic cases of left hemisphere stroke causing aphasia, mostly of ischemic origin, and mostly in men. While certainly not representative of all stroke patients, it is notable that the pattern of results found here closely agrees with various other studies using different samples and methodologies (e.g. Jordan, 2004; Leemburg et al., 2018; Sarasso et al., 2020; van Wijngaarden et al., 2016). For example, EEG delta power increase, alpha slowing and beta suppression have previously been reported even in the acute phase of ischemic stroke (Jordan, 2004). Even so, future work will need to apply the approach used here to a longitudinal dataset to directly compare the acute and chronic stages, and to consider the role of lesion location and etiology in a sample with more diversity in those respects.

While spectral analysis is now commonly employed in research, the first evidence of enhanced slow activity in stroke came from visual inspection of the EEG trace, and this method still plays a role in clinical management of the disease. As such, does the presence of delta activity in the EEG trace contradict our results? We argue that it does not, since the term "delta activity" has historically referred to more than just low frequency periodic oscillations. Rather, pathological delta activity has been characterized as *irregular* when observed from the EEG trace, hence it is occasionally called "polymorphic delta" (Amzica and Steriade, 1998; Gloor et al., 1968; Steriade et al., 1990). This distinction has been largely overlooked in contemporary stroke research that relies on spectral analysis. In other words, this aperiodic pathological delta could consist of slowly changing, high amplitude transient activity, reflective of an increased aperiodic exponent, rather than heightened periodic oscillations. Indeed, as the aperiodic exponent increases, the signal begins to approximate Brown noise ($1/f^2$) – highly autocorrelated noise which produces the perception of slow undulations in the time series, which are nevertheless generated by aperiodic processes (Gilden et al., 1993). To clarify, we do not claim that slow rhythms cannot be affected by stroke, nor that they are unimportant in understanding stroke pathology. Rather, we conclude that the primary driver of the low frequency power that is readily observed in stroke patients, and linked to

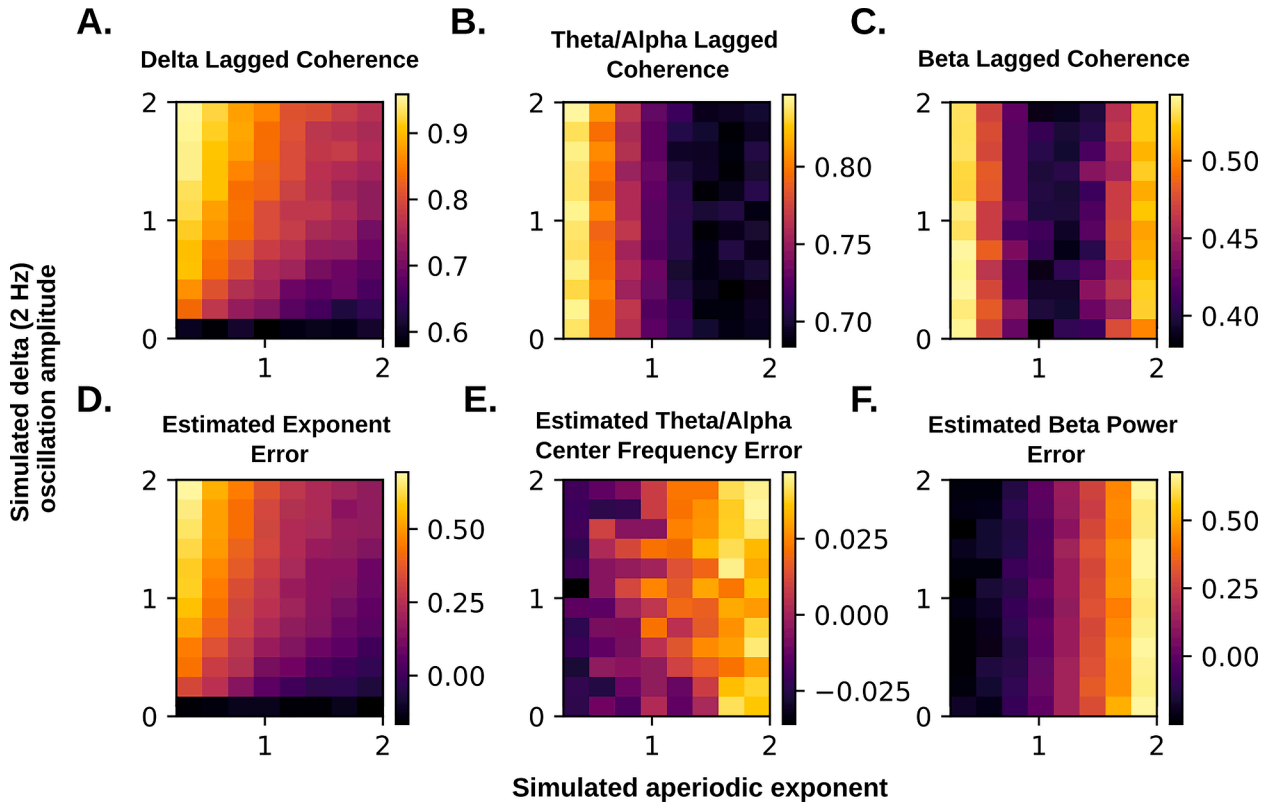

Fig. A1. Simulated signals with systematically varied aperiodic exponent and low frequency (2 Hz) oscillation amplitude reveal biases in lagged coherence (A-C) and specparam (D-F).

patient outcomes, is of aperiodic origin. To further clarify these issues, future work should investigate the interplay between aperiodic exponent and genuine low frequency oscillations, quantifying variation in waveform regularity, and how these may vary from the acute to chronic phases.

Regarding the link between abnormal dynamics and behaviour, we identified a relationship between frequency-domain measures of spectral slowing and cognitive impairment, suggesting that abnormalities in perilesional neural dynamics account for some inter-patient variability in neurocognitive outcomes. Detecting more subtle relationships between behavioural outcomes and abnormal dynamics beyond perilesional tissue will require a larger, more deeply characterized sample to overcome the heterogeneity in lesion location and severity. Similarly, future work should consider patients with more varied behavioural impairments, as it is unclear whether spectral slowing was related to truly domain-general impairment in this sample, or simply aphasia-related difficulties with the linguistic elements common to all tests.

4.6. Conclusions

We have demonstrated that chronic stroke patients exhibit abnormalities in both aperiodic and periodic dynamics, which are most prominent and clearly related to cognitive impairment near the lesion itself, but can also be detected more widely throughout the brain. Notably, the commonly observed elevation in low frequency power was best explained by a steepening of the aperiodic exponent, as no evidence for group differences in low frequency periodic activity were found. We also demonstrated that this aperiodic steepening also covaries with periodic abnormalities, including alpha slowing and beta suppression, suggesting that spectral slowing in stroke patients may be a syndrome comprising multiple types of abnormal electrophysiological features. With this more complete characterization of electrophysiological abnormalities in terms of underlying dynamics, we are better situated to investigate the potential physiological causes and clinical consequences of spectral slowing in stroke. Furthermore, a similar approach can further our understanding of other patient groups known to show spectral slowing, such as those with dementia (Moretti, 2004; Neto et al., 2015), Parkinson's disease (Wiesman et al., 2022), brain tumor (Bosma et al., 2008), and multiple sclerosis (Kim et al., 2019).

5. Ethics Statement

Data collection was conducted in accordance with protocols approved by the Research Ethics Board at Baycrest Health Sciences. All participants gave written informed consent and were compensated for their participation.

Funding

PRJ: Natural Sciences and Engineering Research Council of Canada (NSERC) [CGS-D]; ARM: NSERC [RGPIN-2018-04457]; JAM: Heart and Stroke Foundation Canadian Partnership for Stroke Recovery, Heart and Stroke Foundation Grant in Aid [G-19-0026349], Canada Research Chairs program. Sponsors had no involvement in the study design, data collection, interpretation of results, or decision to pursue publication.

CRediT authorship contribution statement

Phillip R. Johnston: Conceptualization, Methodology, Software, Formal analysis, Visualization, Writing – original draft. **Anthony R. McIntosh:** Methodology, Writing – review & editing, Supervision. **Jed A. Meltzer:** Conceptualization, Methodology, Investigation, Resources, Writing – review & editing, Funding acquisition.

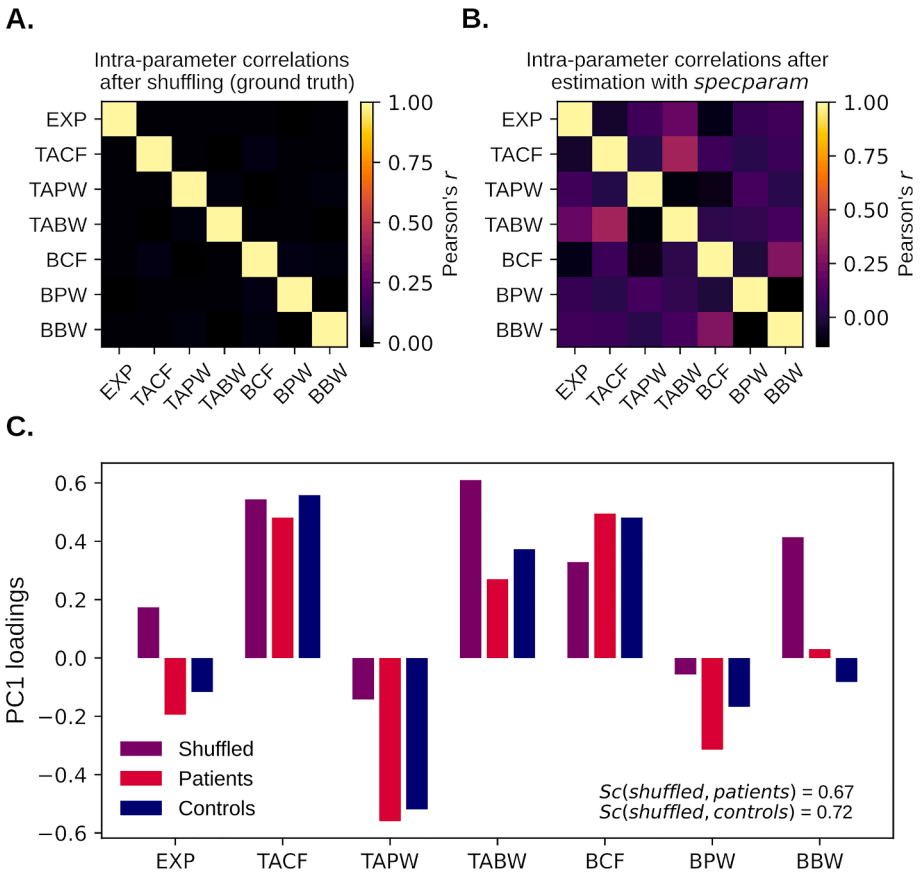

Fig. B1. Applying specparam to simulated spectra with uncorrelated spectral parameters (A) imposes dependencies between parameters (B) that resembles those observed in empirical data (C). Sc = cosine similarity, EXP = aperiodic exponent, TACF/TAPW/TABW = theta-alpha center frequency/power/bandwidth, BCF/BPW/BBW = beta center frequency/power/bandwidth.

Declaration of Competing Interest

The authors declare that they have no known competing financial interests or personal relationships that could have appeared to influence the work reported in this paper.

Data availability

The authors do not have permission to share data.

Appendix A

Simulations were conducted to assess the observed effects in light of biases inherent to lagged coherence and *specparam*. For example, lagged coherence is expected to underestimate rhythmicity at higher aperiodic exponents (i.e. more unpredictability in the signal; Fransen et al., 2015), while *specparam* is expected to overestimate the aperiodic exponent in the presence of large, low frequency oscillations (Gerster et al., 2021). To explore these effects, we computed lagged coherence and *specparam* on simulated power spectra (*specparam*'s fooof.sim.gen(), default parameters, 1–50 Hz) where aperiodic exponent and the amplitude of a delta peak were systematically varied. In addition to variable delta peak and exponent, simulated spectra had peaks of constant size in the alpha range (9 Hz, amplitude 1 unit), and beta range (20 Hz, 0.1 unit).

As expected, estimates of delta rhythmicity decreased as the aperiodic exponent increased (A), however changes in delta rhythmicity remained detectable across all aperiodic exponent values. Therefore, if there was no group difference in aperiodic exponent but rather higher delta oscillations in patients, this would have biased estimated exponent upwards (D) but would still be detectable as increased rhythmicity. We conclude the most likely scenario is that delta oscillations are not higher in patients and aperiodic exponent is, which explains why most patients in fact showed lower estimates of delta rhythmicity compared to controls (Fig. 4A).

Beta rhythmicity estimates were biased upwards at both high and low values of aperiodic exponent (C). It is not clear where the inflection point would fall in real data, so elevated aperiodic exponent could have biased beta rhythmicity upwards or downwards. Given large decreases in *specparam* beta peak power, the most parsimonious explanation remains that beta oscillations are diminished in patients.

Finally, we considered how a difference in aperiodic slope could be responsible for the observed differences in theta-alpha center frequency and beta power. In both cases, biases in specparam estimation were in the opposite direction of the effects observed in patients (E,F), indicating that this was not the case.

Appendix B

To investigate potential dependencies between spectral parameter estimates imposed by the spectral parameterization process, *specparam* was applied to a sample of simulated spectra without correlations between their parameters. Parameter estimates from control participants (aperiodic offset and exponent, theta-alpha center frequency, power and bandwidth, and beta center frequency, power, and bandwidth) were permuted 18,010 times with replacement (10 times the size of the original sample) and used to generate simulated power spectra (*specparam*'s fooof.sim.gen(), default parameters, 1–50 Hz). The resulting power spectra had effectively no correlation between their parameters

(A). As expected, *specparam* applied to these spectra (same settings as described in Methods) produced parameter estimates with non-zero correlations (B). Decomposition of the covariance with PCA produced a first principal component (PC) that resembled the first principal component extracted from both patients and controls (cosine similarity with patient PC1 = 0.67; control PC1 = 0.72) (C) but was less similar to the second principal component (cosine similarity with patient PC2 = 0.34; control PC2 = 0.27), suggesting that this first component may have been an artifact of the parameterization process.

References

Ahmed, I., 1988. Predictive value of the electroencephalogram in acute hemispheric lesions. Clin. EEG Electroencephalogr. 19 (4), 205–209. https://doi.org/10.1177/155005948801900406.

Amzica, F., Steriade, M., 1998. Electrophysiological correlates of sleep delta waves. Electroencephalogr. Clin. Neurophysiol. 107 (2), 69–83. https://doi.org/10.1016/S0013-4694(98)00051-0.

Assenza, G., Zappasodi, F., Squitti, R., Altamura, C., Ventriglia, M., Ercolani, M., Cosimo, C., Lupoi, D., Passarelli, F., Vernieri, F., Maria, P., Tecchio, F., 2009. Neuronal functionality assessed by magnetoencephalography is related to oxidative stress system in acute ischemic stroke. Neuroimage 44 (4), 1267–1273. https://doi.org/10.1016/j.neuroimage.2008.09.049.

Avants, B.B., Tustison, N.J., Song, G., Cook, P.A., Klein, A., Gee, J.C., 2011. A reproducible evaluation of ANTs similarity metric performance in brain image registration. Neuroimage 54 (3), 2033–2044. https://doi.org/10.1016/j.neuroimage.2010.09.025.

Backus, A.R., Schoffelen, J.M., Szebényi, S., Hanslmayr, S., Doeller, C.F., 2016. Hippocampal-prefrontal theta oscillations support memory integration. Curr. Biol. 26 (4), 450–457. https://doi.org/10.1016/j.cub.2015.12.048.

Bosma, I., Stam, C.J., Douw, L., Bartolomei, F., Heimans, J.J., van Dijk, B.W., Postma, T. J., Klein, M., Reijneveld, J.C., 2008. The influence of low-grade glioma on resting state oscillatory brain activity: A magnetoencephalography study. J. Neurooncol 88 (1), 77–85. https://doi.org/10.1007/s11060-008-9535-3.

Carmichael, S.T., 2016. Brain Excitability in Stroke: The Yin and Yang of Stroke. Progression 69, 161–167. https://doi.org/10.1001/archneurol.2011.1175.

Cheyne, D., Bakhtazad, L., Gaetz, W., 2006. Spatiotemporal mapping of cortical activity accompanying voluntary movements using an event-related beamforming approach. Hum. Brain Mapp. 27, 213–229. https://doi.org/10.1002/hbm.20178.

Cheyne, D., Bostan, A.C., Gaetz, W., Pang, E.W., 2007. Event-related beamforming: A robust method for presurgical functional mapping using MEG. Clin. Neurophysiol. 118, 1691–1704. https://doi.org/10.1016/j.clinph.2007.05.064.

Chida, K., Ogasawara, K., Kuroda, H., Aso, K., Kobayashi, M., Fujiwara, S., Yoshida, K., Terasaki, K., Ogawa, A., 2011. Central Benzodiazepine Receptor Binding Potential and CBF Images on SPECT Correlate with Oxygen Extraction Fraction Images on PET in the Cerebral Cortex with Unilateral Major Cerebral Artery Occlusive Disease. J. Nucl. Med. 52, 511–518. https://doi.org/10.2967/jnumed.110.084186.

Chini, M., Pfeffer, T., Hanganu-Opatz, I.L., 2021. *Developmental increase of inhibition drives decorrelation of neural activity* [Preprint]. Neuroscience. https://doi.org/10.1101/2021.07.06.451299.

Cho-Reyes, S., Thompson, C.K., 2012. Verb and sentence production and comprehension in aphasia: Northwestern Assessment of Verbs and Sentences (NAVS). Aphasiology 26 (10), 1250–1277. https://doi.org/10.1080/02687038.2012.693584.

Chu, R.K.O., Braun, A.R., Meltzer, J.A., 2015. Clinical MEG-based detection and localization of perilesional dysfunction in chronic stroke. Neuroimage: Clin. 8, 157–169. https://doi.org/10.1016/j.nicl.2015.03.019.

Clarkson, A.N., Huang, B.S., MacIsaac, S.E., Mody, I., Carmichael, S.T., 2010. Reducing excessive GABA-mediated tonic inhibition promotes functional recovery after stroke. Nature, *V* 468 (7321), 305–309.

Cohen, L., Chaaban, B., Habert, M.-O., 2004. Transient Improvement of Aphasia with Zolpidem. N. Engl. J. Med. 350, 949–950. https://doi.org/10.1056/NEJM200402263500922.

Cohn, R., Mulder, D.W., Neumann, M.A., 1948. Cerebral vascular lesions: electroencephalographic and neuropathologic correlations. Arch. Neurol. Psychiatry 60 (2), 165–181.

Cole, S., Donoghue, T., Gao, R., Voytek, B., 2019. NeuroDSP: A package for neural digital signal processing. Journal of Open Source Software. https://doi.org/10.21105/joss.01272.

Colombo, M.A., Napolitani, M., Boly, M., Gosseries, O., Casarotto, S., Rosanova, M., Brichant, J.-F., Boveroux, P., Rex, S., Laureys, S., Massimini, M., Chieregato, A., Sarasso, S., 2019. The spectral exponent of the resting EEG indexes the presence of consciousness during unresponsiveness induced by propofol, xenon, and ketamine. Neuroimage 189, 631–644. https://doi.org/10.1016/j.neuroimage.2019.01.024.

Cox, R.W., 1996. AFNI: Software for analysis and visualization of functional magnetic resonance. Neuroimages 173 (29), 162–173.

Delis, D.C., Kaplan, E., Kramer, J.H., 2001. Delis-Kaplan Executive Function System (D–KEFS). APA PsycTests. https://doi.org/10.1037/t15082-000.

Destexhe, A., Contreras, D., Steriade, M., 1999. Spatiotemporal analysis of local field potentials and unit discharges in cat cerebral cortex during natural wake and sleep states. J. Neurosci. 19 (11), 4595–4608. https://doi.org/10.1523/JNEUROSCI.19-11-04595.1999.

Dong, Y., Fukuyama, H., Nabatame, H., Yamauchi, H., Shibasaki, H., Yonekura, Y., 1997. Assessment of Benzodiazepine Receptors Using Iodine-123–Labeled Iomazenil Single-Photon Emission Computed Tomography in Patients With Ischemic Cerebrovascular Disease: A Comparison With PET Study. Stroke 28, 1776–1782. https://doi.org/10.1161/01.STR.28.9.1776.

Donoghue, T., Haller, M., Peterson, E.J., Varma, P., Sebastian, P., Gao, R., Noto, T., Lara, A.H., Wallis, J.D., Knight, R.T., Shestyuk, A., Voytek, B., 2020. Parameterizing neural power spectra into periodic and aperiodic components. Nat. Neurosci. 23 (12), 1655–1665. https://doi.org/10.1038/s41593-020-00744-x.

Donoghue, T., Schaworonkow, N., Voytek, B., 2021. Methodological considerations for studying neural oscillations. Eur. J. Neurosci. https://doi.org/10.1111/ejn.15361.

Dunn, M., Dunn, L., 1997. Peabody Picture Vocabulary Test. AGS, London.

Engel, A.K., Fries, P., 2010. Beta-band oscillations—Signalling the status quo? Curr. Opin. Neurobiol. 20 (2), 156–165. https://doi.org/10.1016/j.conb.2010.02.015.

Feeney, D.M., Baron, J.-C., 1986. Diaschisis. Stroke 17, 817–830.

Finger, S., Kochler, P.J., Jagella, C., 2004. The Monakow Concept of Diaschisis. Hist. Neurol 61, 283–288.

Finnigan, S., van Putten, M.J.A.M., 2013. EEG in ischaemic stroke: Quantitative EEG can uniquely inform (sub-)acute prognoses and clinical management. Clin. Neurophysiol. 124 (1), 10–19. https://doi.org/10.1016/j.clinph.2012.07.003.

Fransen, A.M.M., Ede, F.V., Maris, E., 2015. Identifying neuronal oscillations using rhythmicity. Neuroimage 118, 256–267. https://doi.org/10.1016/j.neuroimage.2015.06.003.

Freeman, W.J., Zhai, J., 2009. Simulated power spectral density (PSD) of background electrocorticogram (ECoG). Cogn. Neurodyn. 3, 97–103. https://doi.org/10.1007/s11571-008-9064-y.

Gao, R., Peterson, E.J., Voytek, B., 2017. Inferring synaptic excitation/inhibition balance from field potentials. Neuroimage 158 (June), 70–78. https://doi.org/10.1016/j.neuroimage.2017.06.078.

Gerster, M., Waterstraat, G., Litvak, V., Lehnertz, K. 2021. *Separating neural oscillations from aperiodic 1/f activity: Challenges and recommendations*. 0–45.

Giaquinto, S., Cobianchi, A., Macera, F., Nolfe, G., 1994. EEG recordings in the course of recovery from stroke. Stroke 25 (11), 2204–2209.

Gilden, D. L., Schmuckler, M. A., Clayton, K. (1993). *The perception of natural contour*. 19.

Gloor, P., Kalabay, O., Giard, N., 1968. The electroencephalogram in diffuse encephalopathies: electroencephalographic correlates of grey and white matter lesions. Brain 91 (4), 779–802. https://doi.org/10.1093/brain/91.4.779.

Hall, S.D., Yamawaki, N., Fisher, A.E., Clauss, R.P., Woodhall, G.L., Stanford, I.M., 2010. GABA(A) alpha-1 subunit mediated desynchronization of elevated low frequency oscillations alleviates specific dysfunction in stroke – A case report. Clin. Neurophysiol. 121, 549–555. https://doi.org/10.1016/j.clinph.2009.11.084.

He, B.J., 2011. Scale-free properties of the functional magnetic resonance imaging signal during rest and task. J. Neurosci. 31 (39), 13786–13795. https://doi.org/10.1523/JNEUROSCI.2111-11.2011.

He, B.J., 2014. Scale-free brain activity: Past, present, and future. Trends Cogn. Sci. 18 (9), 480–487. https://doi.org/10.1016/j.tics.2014.04.003.

He, B.J., Zempel, J.M., Snyder, A.Z., Raichle, M.E., 2010. The temporal structures and functional significance of scale-free brain activity. Neuron 66 (3), 353–369. https://doi.org/10.1016/j.neuron.2010.04.020.

Hochberg, Y., Tamhane, A.C., 1987. Multiple Comparison Procedures, Wiley Series in Probability and Statistics. John Wiley & Sons, Inc. https://doi.org/10.1002/9780470316672.

Huang, M.X., Mosher, J.C., Leahy, R.M., 1999. A sensor-weighted overlapping-sphere head model and exhaustive head model comparison for MEG. Phys. Med. Biol. 44 (2), 423–440.

Jones, S.R., 2016. When brain rhythms aren't 'rhythmic': Implication for their mechanisms and meaning. Curr. Opin. Neurobiol. 40, 72–80. https://doi.org/10.1016/j.conb.2016.06.010.

Jordan, K.G., 2004. Emergency EEG and continuous EEG monitoring in acute ischemic stroke. J. Clin. Neurophysiol. 21 (5), 12.

Josse, J., Pagès, J., Husson, F., 2011. Multiple imputation in principal component analysis. Adv. Data Anal. Classif. 5, 231–246. https://doi.org/10.1007/s11634-011-0086-7.

Juhasz, C., Kamondi, A. 1997. *Spectral EEG analysis following hemispheric stroke Evidences of transhemispheric diaschisis*. 397–400.

Kaplan, P.W., Rossetti, A.O., 2011. EEG patterns and imaging correlations in encephalopathy. Encephalopathy Part 28 (3), 233–251.

Kaplan, E., Goodglass, H. & Weintraub, S. Boston Naming Test (Lea & Febiger, London, 2001).

Kertesz, A., 1982. The Western Aphasia Battery. Grune & Stratton, New York.

Kielar, A., Deschamps, T., Chu, R.K.O., Jokel, R., Khatamian, Y.B., Chen, J.J., Meltzer, J. A., 2016. Identifying dysfunctional cortex: Dissociable effects of stroke and aging on resting state dynamics in MEG and fmri. Front. Aging Neurosci. 8 (MAR) https://doi.org/10.3389/fnagi.2016.00040.

Kim, J.A., Bosma, R.L., Hemington, K.S., Rogachov, A., Osborne, N.R., Cheng, J.C., Oh, J., Crawley, A.P., Dunkley, B.T., Davis, K.D., 2019. Neuropathic pain and pain interference are linked to alpha-band slowing and reduced beta-band magnetoencephalography activity within the dynamic pain connectome in patients with multiple sclerosis. Pain 160 (1), 187–197. https://doi.org/10.1097/j.pain.0000000000001391.

Kirsch, H.E., Robinson, S.E., Mantle, M., Nagarajan, S., 2006. Automated localization of magnetoencephalographic interictal spikes by adaptive spatial filtering. Clin. Neurophysiol. 117, 2264–2271. https://doi.org/10.1016/j.clinph.2006.06.708.

Laaksonen, K., Helle, L., Parkkonen, L., Kirveskari, E., Mäkelä, J.P., Mustanoja, S., Tatlisumak, T., Kaste, M., Forss, N., Chacron, M.J., 2013. Alterations in spontaneous brain oscillations during stroke recovery. PloS ONE 8 (4), e61146.

Lane, D. (2010). Tukey's honestly significant difference (HSD). In *Encyclopedia of Research Design* (pp. 1565–1570). SAGE. https://books.scholarsportal.info/uri/ebooks/ ebooks3/sage/2016-09-07/2/9781412961271v3.

Lanzone, J., Colombo, M.A., Sarasso, S., Zappasodi, F., Rosanova, M., Massimini, M., Di Lazzaro, V., Assenza, G., 2022. EEG spectral exponent as a synthetic index for the longitudinal assessment of stroke recovery. Clin. Neurophysiol. 137, 92–101. https://doi.org/10.1016/j.clinph.2022.02.022.

Law, R.G., Pugliese, S., Shin, H., Sliva, D.D., Lee, S., Neymotin, S., Moore, C., Jones, S.R., 2022. Thalamocortical mechanisms regulating the relationship between transient beta events and human tactile perception. Cereb. Cortex 32, 668–688.

Leach, L., Kaplan, E., Rewilak, D., Richards, B., & Proulx, G.B. Kaplan Baycrest Neurocognitive Assessment: Manual (Pearson, 2000).

Leemburg, S., Gao, B., Cam, E., Sarnthein, J., Bassetti, C.L., 2018. Power spectrum slope is related to motor function after focal cerebral ischemia in the rat. Sleep 41 (10), 1–12. https://doi.org/10.1093/sleep/zsy132.

Lendner, J.D., Helfrich, R.F., Mander, B.A., Romundstad, L., Lin, J.J., Walker, M.P., Larsson, P.G., Knight, R.T., 2020. An electrophysiological marker of arousal level in humans. Elife 9, e55092.

Lombardi, F., Herrmann, H.J., de Arcangelis, L., 2017. Balance of excitation and inhibition determines 1/f power spectrum in neuronal networks. *Chaos: An Interdisciplinary*. J. Nonlinear Sci. 27 (4), 047402 https://doi.org/10.1063/1.4979043.

Lopes da Silva, F.H., Vos, J.E., Mooibroek, J., van Rotterdam, A., 1980. Relative contributions of intracortical and thalamo-cortical processes in the generation of alpha rhythms, revealed by partial coherence analysis. Electroencephalogr. Clin. Neurophysiol. 50 (5–6), 449–456. https://doi.org/10.1016/0013-4694(80)90011-5.

Machado, C., Cuspineda, E., Valdés, P., Virues, T., Liopis, F., Bosch, J., Aubert, E., Hernández, E., Pando, A., Álvarez, M.A., Barroso, E., Galán, L., Avila, Y., 2004. Assessing acute middle cerebral artery ischemic stroke by quantitative electric tomography. Clin. EEG Neurosci. 35 (3), 116–124.

Macwhinney, B., Fromm, D., Forbes, M., Holland, A., 2011. AphasiaBank: Methods for Studying Discourse. Aphasiology 25 (11), 1286–1307. https://doi.org/10.1080/02687038.2011.589893.

McIntosh, A.R., Lobaugh, N.J., 2004. Partial least squares analysis of neuroimaging data: Applications and advances. Neuroimage 23, 250–263. https://doi.org/10.1016/j.neuroimage.2004.07.020.

Meinzer, M., Flaisch, T., Breitenstein, C., Wienbruch, C., Elbert, T., Rockstroh, B., 2008. Functional re-recruitment of dysfunctional brain areas predicts language recovery in chronic aphasia. Neuroimage 39 (4), 2038–2046. https://doi.org/10.1016/j.neuroimage.2007.10.008.

Moretti, D., 2004. Individual analysis of EEG frequency and band power in mild Alzheimer's disease. Clin. Neurophysiol. 115 (2), 299–308. https://doi.org/10.1016/S1388-2457(03)00345-6.

Murri, L., Gori, S., Massetani, R., Bonanni, E., Marcella, F., Milani, S., 1998. Evaluation of acute ischemic stroke using quantitative EEG: A comparison with conventional EEG and CT scan. Neurophysiol. Clin. 28 (3), 249–257. https://doi.org/10.1016/S0987-7053(98)80115-9.

Nagata, K., Mizukami, M., Araki, G., Kawase, T., Hirano, M., 1982. Topographic electroencephalographic study of cerebral infarction using computed mapping of the EEG. J. Cereb. Blood Flow Metab. 2 (1), 79–88. https://doi.org/10.1038/jcbfm.1982.9.

Nagata, K., Tagawa, K., Hiroi, S., Shishido, F., Uemura, K., 1989. Electroencephalographic correlates of blood flow and oxygen metabolism provided by positron emission tomography in patients with cerebral infarction. Electroencephalogr. Clin. Neurophysiol. 72 (1), 16–30. https://doi.org/10.1016/0013-4694(89)90027-8.

Neto, E., Allen, E.A., Aurlien, H., Nordby, H., Eichele, T., 2015. EEG spectral features discriminate between Alzheimer's and vascular dementia. Front. Neurol. 6 https://doi.org/10.3389/fneur.2015.00025.

Orfila, J.E., Grewal, H., Dietz, R.M., Strnad, F., Shimizu, T., Moreno, M., Schroeder, C., Yonchek, J., Rodgers, K.M., Dingman, A., Bernard, T.J., Quillinan, N., Macklin, W.B., Traystman, R.J., Herson, P.S., 2019. Delayed inhibition of tonic inhibition enhances functional recovery following experimental ischemic stroke. J. Cereb. Blood Flow Metab. 39 (6), 1005–1014. https://doi.org/10.1177/0271678X17750761.

Podvalny, E., Noy, N., Harel, M., Bickel, S., Chechik, G., Schroeder, C.E., Mehta, A.D., Tsodyks, M., Malach, R., 2015. A unifying principle underlying the extracellular field potential spectral responses in the human cortex. J. Neurophysiol. 114 (1), 505–519. https://doi.org/10.1152/jn.00943.2014.

Pritchard, W.S., 1992. The brain in fractal time: 1/f-like power spectrum scaling of the human electroencephalogram. Int. J. Neurosci. 66, 119–129. https://doi.org/10.1080/1071441950170102.

Rossiter, H.E., Davis, E.M., Clark, E.V., Boudrias, M.-H., Ward, N.S., 2014. Beta oscillations reflect changes in motor cortex inhibition in healthy ageing. Neuroimage 91, 360–365. https://doi.org/10.1016/j.neuroimage.2014.01.012.

Rowe, D.L., Robinson, P.A., Rennie, C.J., 2004. Estimation of neurophysiological parameters from the waking EEG using a biophysical model of brain dynamics. J. Theor. Biol. 231 (3), 413–433.

Sarasso, S., Ambrosio, S. D., Fecchio, M., Casarotto, S., Landi, C., Mattavelli, G., Gosseries, O., Quarenghi, M., Laureys, S., Devalle, G., Rosanova, M., Massimini, M. (2020). Local sleep-like cortical reactivity in the awake brain after focal injury. *Brain*, 3672–3684. 10.1093/brain/awaa338.

Seabold, S., Perktold, J., 2010. Statsmodels: Econometric and Statistical Modeling with Python. Proceedings of the Python in Science Conference. https://doi.org/10.25080/majora-92bf1922-011.

Shah-Basak, P.P., Kielar, A., Deschamps, T., Verhoeff, N.P., Jokel, R., Meltzer, J., 2018. Spontaneous oscillatory markers of cognitive status in two forms of dementia. Hum. Brain Mapp. 1–14. https://doi.org/10.1002/hbm.24470.

Shah-Basak, P.P., Sivaratnam, G., Teti, S., Francois-Nienaber, A., Yossofzai, M., Armstrong, S., Nayar, S., Jokel, R., Meltzer, J., 2020. High definition transcranial direct current stimulation modulates abnormal neurophysiological activity in post-stroke aphasia. Sci. Rep. 10 (1), 1–18. https://doi.org/10.1038/s41598-020-76533-0.

Signorino, M., Pucci, E., Belardinelli, N., Nolfe, G., Angeleri, F., 1995. EEG spectral analysis in vascular and Alzheimer dementia. Electroencephalogr. Clin. Neurophysiol. 94 (5), 313–325. https://doi.org/10.1016/0013-4694(94)00290-2.

Spitzer, B., & Haegens, S. (2017). Beyond the status quo: A Role for beta oscillations in endogenous content (re)activation. *Eneuro*, *4*(4), ENEURO.0170-17.2017. 10.1523/ENEURO.0170-17.2017.

Steriade, M., Gloor, P., Llinás, R.R., Lopes da Silva, F.H., Mesulam, M.-M., 1990. Basic mechanisms of cerebral rhythmic activities. Electroencephalogr. Clin. Neurophysiol. 76 (6), 481–508. https://doi.org/10.1016/0013-4694(90)90001-Z.

Tecchio, F., Zappasodi, F., Pasqualetti, P., Tombini, M., Salustri, C., Oliviero, A., Pizzella, V., Vernieri, F., Rossini, P.M., 2005. Rhythmic brain activity at rest from rolandic areas in acute mono-hemispheric stroke: A magnetoencephalographic study. Neuroimage 28 (1), 72–83. https://doi.org/10.1016/j.neuroimage.2005.05.051.

Tecchio, F., Pasqualetti, P., Zappasodi, F., Tombini, M., Lupoi, D., Vernieri, F., Rossini, P. M., 2007. Outcome prediction in acute monohemispheric stroke via magnetoencephalography. J. Neurol. 254 (3), 296–305. https://doi.org/10.1007/s00415-006-0355-0.

Trakoshis, S., Canella, C., You, W., Chakrabarti, B., Ruigrok, A.N., Bullmore, E.T., Suckling, J., Markicevic, M., Zerbi, V., Lai, M.-C., Panzeri, S., Lombardo, M.V., 2020. Intrinsic excitation-inhibition imbalance affects medial prefrontal cortex differently in autistic men versus women. Neurosci. Med. 9 (e55684), 31.

Tzourio-Mazoyer, N., Landeau, B., Papathanassiou, D., Crivello, F., Etard, O., Delcroix, N., Mazoyer, B., Joliot, M., 2002. Automated anatomical labeling of activations in SPM using a macroscopic anatomical parcellation of the MNI MRI single-subject brain. Neuroimage 15 (1), 273–289. https://doi.org/10.1006/nimg.2001.0978.

van Wijngaarden, J.B.G., Zucca, R., Finnigan, S., Verschure, P.F.M.J., 2016. The impact of cortical lesions on thalamo-cortical network dynamics after acute ischaemic stroke: A combined experimental and theoretical study. PLoS Comput. Biol. 12 (8), 1–16. https://doi.org/10.1371/journal.pcbi.1005048.

Vrba, J., Robinson, S.E., 2001. Signal processing in magnetoencephalography. Methods 25 (2), 249–271. https://doi.org/10.1006/meth.2001.1238.

Waschke, L., Donoghue, T., Fiedler, L., Smith, S., Garrett, D.D., Voytek, B., Obleser, J., 2021. Modality-specific tracking of attention and sensory statistics in the human electrophysiological spectral exponent. eLife 10, e70068.

Wiesman, A.I., da Silva Castanheira, J., Baillet, S., 2022. Stability of spectral estimates in resting-state magnetoencephalography: Recommendations for minimal data duration with neuroanatomical specificity. Neuroimage 247, 118823. https://doi.org/10.1016/j.neuroimage.2021.118823.

Wiesman, A.I., da Silva Castanheira, J., Degroot, C., Fon, E.A., Baillet, S., Prevent-AD Research Group, Quebec Parkinson Network, 2022. A sagittal gradient of pathological and compensatory effects of neurophysiological slowing in Parkinson's disease [Preprint]. Neurology. https://doi.org/10.1101/2022.08.05.22278436.

Wilkinson, L., 1999. Statistical Methods in Psychology Journals. Am. Psychol. 11.

Wu, J., Srinivasan, R., Burke Quinlan, E., Solodkin, A., Small, S.L., Cramer, S.C., 2016. Utility of EEG measures of brain function in patients with acute stroke. J. Neurophysiol. 115 (5), 2399–2405. https://doi.org/10.1152/jn.00978.2015.

Zappasodi, F., Olejarczyk, E., Marzetti, L., Assenza, G., Pizzella, V., Tecchio, F. 2014. Fractal dimension of EEG activity senses neuronal impairment in acute stroke. *PLoS ONE*, *9*(6), e100199. 10.1371/journal.pone.0100199.

Zappasodi, F., Tombini, M., Milazzo, D., Rossini, P.M., Tecchio, F., 2007. Delta dipole density and strength in acute monohemispheric stroke. Neurosci. Lett. 416 (3), 310–314.